1950

Fighter aircraft fire control system with improved components

Freeman, William B.; Thompson, Allen B.; Wilson, Carter L.

Massachusetts Institute of Technology

Report No. 6411-T-1

FIGHTER AIRCRAFT FIRE CONTROL SYSTEM WITH IMPROVED COMPONENTS

By

William B. Freeman
Allen B. Thompson
Carter L. Wilson, Jr.

UNCLASSIFIED

PUBLISHED BY

INSTRUMENTATION LABORATORY

MASSACHUSETTS INSTITUTE OF TECHNOLOGY

Cambridge 39. Mass.

UNITED STATES AIR FORCE
AIR MATERIEL COMMAND
ENGINEERING FIELD OFFICER
MASSACHUSETTS INSTITUTE OF TECHNOLOGY
CAMBRIDGE 39, MASS.

M E M O R A N D U M

MCREOL-18/JDA/mlb
18 August 1950

SUBJECT: Technical Publication, Approval of

TO: U. S. Naval Post Graduate School
U. S. Naval Academy
Annapolis, Maryland

1. Your attention is invited to the fact that Instrumentation Laboratory Report 6411-T-1 is a thesis study prepared by students under the supervision of the Instrumentation Laboratory, but does not necessarily have the approval of the laboratory.

2. In view of this fact, it is suggested that no action which is based on conclusions and recommendations of that thesis be taken without further consultation with the Director of the Instrumentation Laboratory.

3. The Institute is now conducting studies concerning the conclusions and recommendations contained in Report 6411-T-1 and will issue a memorandum containing the official Instrumentation Laboratory recommendations on the subject concerned.

J. D. ARONSON
AMC Engineering Field Officer

RESTRICTED

FIGHTER AIRCRAFT FIRE CONTROL SYSTEM WITH IMPROVED COMPONENTS

by

WILLIAM B. FREEMAN

ALLEN B. THOMPSON

CARTER L. WILSON, JR.

SUBMITTED IN PARTIAL FULFILLMENT OF THE

REQUIREMENTS FOR THE DEGREE OF

MASTER OF SCIENCE

at

MASSACHUSETTS INSTITUTE OF TECHNOLOGY

1950

May 19, 1950

Prof. Joseph S. Newell
Secretary of the Faculty
Massachusetts Institute of Technology
Cambridge 39, Massachusetts

Dear Professor Newell:

In accordance with the regulations of the faculty, we hereby submit a thesis entitled, FIGHTER AIRCRAFT FIRE CONTROL SYSTEM WITH IMPROVED COMPONENTS, in partial fulfillment of the requirements for the degree of Master of Science.

ABSTRACT

The A-1 Fighter Sight was developed by the Instrumentation Laboratory of the Massachusetts Institute of Technology, utilizing conventional single-degree-of-freedom gyros and mechanical computers.

Since the development of the A-1 Sight, the Instrumentation Laboratory has developed a new type of single-degree-of-freedom gyro and a mechanical computer unit whose accuracy, durability and dependability are superior to any in current use.

This thesis presents analyses of two system configurations which utilized the new components.

The first configuration, referred to as System Number 1, consisted of the gyro unit alone and utilized the gimbal shaft of the gyro as a computer shaft. The characteristic equation was of first order. This system proved to be excellent for generation of prediction angle, but with the equipment used in the laboratory it was unsatisfactory for tracking. An analytical study showed that the system would be satisfactory from both prediction and tracking points of view when the damping coefficient of the gyro was increased.

The second configuration, referred to as System Number 2, consisted of both a gyro and a computer unit. The gyro was first considered to receive the angular velocity of the control line and, with the computer and other components, generate prediction angle. For this operation, damping was insufficient to give satisfactory performance. The effect of added damping and the effect of adding a lead network to exactly cancel the lag introduced by the gyro were studied both analytically and with a Philbrick electronic simulator. As in the case of System Number 1, additional damping resulted in a satisfactory system. Second, in an analytical study, the gyro was used in a fully automatic system for both stabilization and for use in generating prediction angle.

With the gyro modified to obtain more damping, System Number 1 would be satisfactory as a replacement for the elevation channel of the A-1 Sight. For manual tracking, System Number 2 would also be satisfactory with additional damping. System Number 2 is also satisfactory as a component of a fully automatic system.

ACKNOWLEDGEMENT

The authors wish to express their deep appreciation to Dr. C. S. Draper, Prof. D. Amara, Mr. C. Haskell and Mr. J. R. Rogers for the interest, encouragement and assistance given them in the supervision of this thesis and in making available the facilities and equipment of the Instrumentation Laboratory.

Invaluable aid was given by Mr. L. D. Richardson, Mr. J. P. Anderson, Mr. R. L. Wales and Mr. M. M. Bittel in proposing component calibration techniques and in supervising alignment of equipment.

Thanks are also extended to Mr. G. J. Coury for technical assistance.

Thanks are given to Mr. L. E. Payne and his associates of Jackson & Moreland for their part in the preparation of the text and illustrations.

The graduate work, for which this thesis is a partial requirement, was performed while the authors were assigned to Naval Training School, Massachusetts Institute of Technology. This thesis was prepared under the auspices of D.I.C. Project 6411, sponsored by the Office of Air Research and the Armament Laboratory, Engineering Division, Air Materiel Command, through Contract Mx-402, Project W 33-038-ac-13969.

TABLE OF CONTENTS

CHAPTER I

INTRODUCTION

Beginning in 1945, the Instrumentation Laboratory of the Massachusetts Institute of Technology developed a series of single-degree-of-freedom gyro units and mechanical computer units whose durability, accuracy, and compactness are far superior to those now in service. The gyro units with microsyn pickoff and torque generator, and the computers with microsyn units for pickoff, elastic restraint, and torque generation are packaged in hermetically sealed, temperature-stabilized containers. Case damping is present in both the gyro and the computer units.

Present day fighter aircraft operations take place under conditions in which the temperature may vary from 120°F to -60°F, and the humidity may vary from virtually none to 100% in the space of a very few minutes. These operations occur in all types of environment from that of carrier decks to desert airfields.

In view of the fact that the new components have fewer uncertainties than those in current use, and that their performance and durability are not affected by dust, humidity, or temperature changes, it was considered desirable to investigate the possibility of incorporating them in a redesign of the A-1 Lead-Computing Fighter Gunsight.

The A-1 Sight is described in a report entitled "Detailed Theory and Computations for the A-1 Sight for the Control of Gunfire from Fixed Guns, Rocketfire, and Bombing from Aircraft", Volumes I and II, together with a complete analysis of the fire control problem mechanized. In this study, no attempt was made to create and analyze additional fire control problems, but rather to investigate the improvement in performance of the A-1 Sight resulting from use of these newly developed components.

For the study, two system configurations were employed. The first, an analysis of which appears in Chapter II, utilized a gyro unit alone with computations being made directly on the gimbal shaft. The theory and operation of such a system is fully described in "Detailed Theory and Computations for the Control of Gunfire from Fixed Guns, Rocketfire, and Bombing from Aircraft". The second system configuration was so arranged that the gyro could either be used to receive angular velocity of the control line as an input and operate with the remaining components to generate prediction angle, or be used in a fully automatic system for both stabilization and generation of prediction angle. An analysis of this second configuration appears in Chapter III.

Limitations were imposed by the fact that the equipment employed in this study consisted of components already in existence, and no attempt was made to tailor equipment to the problem. However, with this equipment, it was possible to prove the principles involved and to determine design specifications of components required for a production configuration. The equipment used in this study is described in Appendix A.

This investigation was restricted to the elevation channel, due to limited time and equipment availability.

CHAPTER II

SYSTEM USING GYRO ONLY

1. Introduction

In the elevation channel of the A-1 Sight, as described in reference (1), torque as such was transmitted through the gyro linkage to a separate computer shaft. Torques were summed on this computer shaft, and a voltage corresponding to the resultant angle was picked off and fed into the indicating system. A functional diagram of this arrangement is shown on Fig. II-1.

Since the single-degree-of-freedom gyro had a signal generator and a torque generator mounted on the gimbal shaft, it was considered advisable to investigate the possibility of summing torques there, ie., using the gimbal shaft of the gyro as the computer. Accordingly, that configuration whose functional diagram appears on Fig. II-2 was set up in the laboratory.

Description and performance of the components appears in Appendix A.

It may be noted that the only inputs to the system of Fig. II-2 are range and angular velocity of the control line. In a final or production configuration, altitude and superelevation would be additional inputs. Since appropriate networks were not available and since the principle of the configuration could be proved without them, these inputs were not introduced.

2. Equations for the System.

For the system of Fig. II-2, the following equations were obtained:

$$M_g = M_{tg} + C_g \dot{A}_g \tag{II-1}$$

$$W_{CL}\, S_{g\ W;M} = i^2_{(tg)}\, S_{(tg)}[i^2;M] + C_g \dot{A}_g \tag{II-2}$$

$$e_{sg} = A_g\, S_{(sg)}[A;e] \tag{II-3}$$

$$i^2_{(tg)} = S_{(tg\ \ amp)}[e;i^2]\ {}^{e}R_o$$

$$= S_{(tg\ \ amp)}[e;i^2]\ S_{R_o}[e;e]$$

$$S_{(amp)}[e;e]\ S_{(sg)}[A;e]\ A_g \tag{II-4}$$

Substituting (II-4) in (II-2),

$$W_{CL}\, S_{g[W;M]} = S_{(tg)}[i^2;M]\ S_{(tg\ \ amp)\ e;i^2}\ S_{R_o}[e;e]$$

$$S_{(amp)}[e;e]\ S_{(sg)}[A;e]\ A_g + C_g \dot{A}_g \tag{II-5}$$

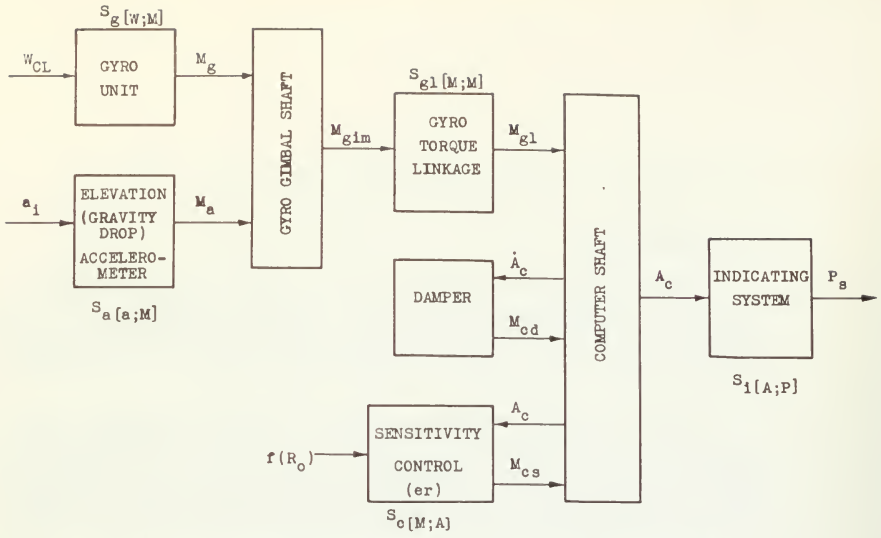

FIG. II-1. FUNCTIONAL DIAGRAM OF A-1 SIGHT ELEVATION CHANNEL.

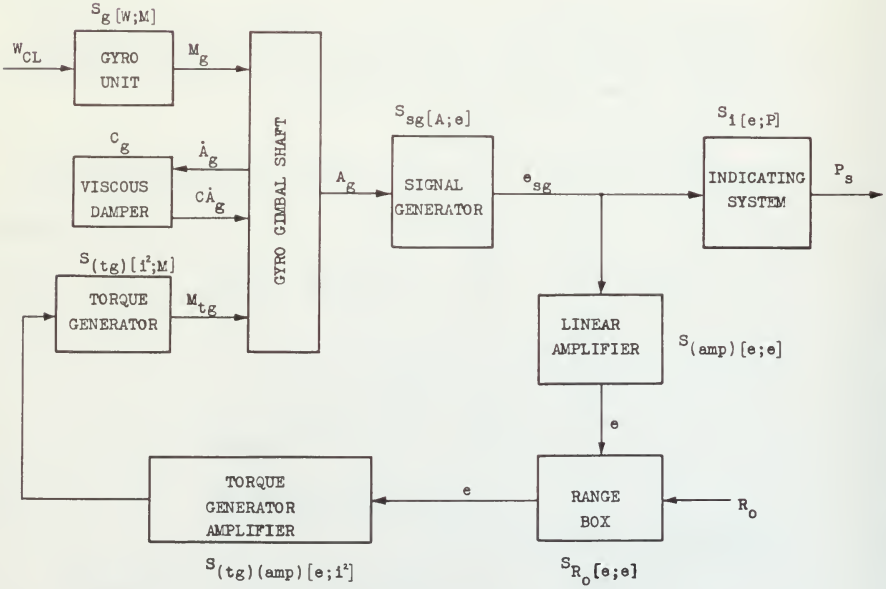

FIG. II-2. FUNCTIONAL DIAGRAM OF SYSTEM NO. 1.

Defining $S_{(er)[A;M]}$

$$S_{(er)[A;M]} = S_{(tg)[i^2;M]}\, S_{(tg\ \ amp)[e;i^2]}\, S_{R_o[e;e]}\, S_{(amp)[e;e]}\, S_{(sg)[A;e]} \qquad \text{(II-5a)}$$

$$\frac{C_g}{S_{(er)[A;M]}}\,\dot{A}_g + A_g = \frac{S_{g[W;M]}}{S_{(er)[A;M]}}\, W_{CL} \qquad \text{(II-6)}$$

$$P_s = S_{i[e;P]}\, e_{sg} = S_{i[A;P]}\, A_g \qquad \text{(II-7)}$$

$$\dot{P}_s = S_{i[A;P]}\, \dot{A}_g \qquad \text{(II-8)}$$

From (II-7) and (II-8)

$$\left.\begin{aligned} A_g &= \frac{P_s}{S_{i[A;P]}} \\ \dot{A}_g &= \frac{\dot{P}_s}{S_{i[A;P]}} \end{aligned}\right\}. \qquad \text{(II-9)}$$

(II-9) in (II-6),

$$\frac{C_g}{S_{(er)[A;M]}}\,\dot{P}_s + P_s = \frac{S_{g[W;M]}\, S_{i[A;P]}}{S_{(er)[A;M]}}\, W_{CL} \qquad \text{(II-10)}$$

Define:

$$\frac{C_g}{S_{(er)[A;M]}} = (CT)_g \quad , \qquad \text{(II-10a)}$$

$$\frac{S_{g[W;M]}\, S_{i[A;P]}}{S_{(er)[A;M]}} = S_{p[W;P]} \qquad \text{(II-10b)}$$

and substituting in (II-10)

$$(CT)_g \dot{P}_s + P_s = S_{p[W;P]} W_{CL} , \qquad \text{(II-11)}$$

from which

$$\frac{P_s}{W_{CL}} = \frac{S_{p[W;P]}}{[(CT)_g p + 1]} \qquad \text{(II-12)}$$

Defining stability number,

$$(SN) = \left[\frac{(CT)_g}{S_{p[W;P]}} - 1 \right] , \qquad \text{(II-13)}$$

(II-12) becomes

$$\frac{P_s}{W_{CL}} = \frac{S_{p[W;P]}}{[1 + [(SN) + 1] S_{p[W;P]} p]} \qquad \text{(II-14)}$$

$$W_{CL} = W_{TL} + \dot{P}_s \qquad \text{(II-15)}$$

Substituting (II-15) in (II-12),

$$P_s = \frac{S_{p[W;P]} (W_{TL} + \dot{P}_s)}{[1 + (CT)_g p]}$$

$$P_s \left[1 - \frac{S_{p[W;P]} p}{1 + (CT)_g p}\right] = \frac{S_{p[W;P]} W_{TL}}{[1 + (CT)_g p]}$$

from which,

$$\frac{P_s}{W_{TL}} = \frac{S_{p[W;P]}}{1 + (SN) S_{p[W;P]} p} \qquad \text{(II-16)}$$

Combining (II-14) and (II-16)

$$\text{Tracking Ratio} = TR = \frac{CL}{TL} = \frac{W_{CL}}{W_{TL}} = \frac{1 + [(SN) + 1] S_{p[W;P]} p}{1 + (SN) S_{p[W;P]} p} \qquad \text{(II-17)}$$

3. Description of Laboratory Setup.

A power pack for supplying 400 cps current for signal generator excitation and 400 cps, 3 phase voltage for driving the gyro wheel was obtained by using a 400 cps fork, a linear amplifier and a phase splitting network, the circuit diagram of which is shown on Fig. II-3. The 3 phase voltage was controlled by the gain of the linear amplifier, and was set at 12 volts, as recommended for the gyro wheel drive. The output from the fork was run through a phasing network and a second linear amplifier for exciting the signal generators.

The single-degree-of-freedom gyro was mounted on a rate table, with which angular velocities of the control line could be simulated. The output from the signal generator was fed through a third linear amplifier into the range box. The range box was simply a potentiometer, with the wiper position calibrated for range as described below. The output from the range box was fed into the torque generator amplifier, whose output energized the torque generator on the gimbal shaft.

The output of the first linear amplifier was used as a reference voltage in the torque generator amplifier. The excitation to the signal generator was phased with this reference voltage by means of the phasing network mentioned above.

The output from the signal generator on the gimbal shaft was also fed into the indicating system of the A-1 Sight. This indicating system consisted of the servo amplifier and sight head, as described in reference (1).

Reference voltage to the servo amplifier of the A-1 Sight was obtained from the gyro wheel drive. It was fed into the stator of an autosyn, and the output of the autosyn was amplified to 28 volts. The signal generator in the sight head was excited in series with that on the gyro gimbal shaft, and the reference voltage was phased with the sight head signal generator output by rotating and locking the rotor of the autosyn.

4. Determination and Adjustment of Sensitivities.

Certain of the system sensitivities were determined in the manner described in Appendix A. They are:

$$S_{g[W;M]} = .1 \times 10^6 \text{ dyne-cm-sec/radian} \qquad \text{(II-18)}$$

$$S_{(sg)[A;e]} = 32 \text{ mv/mr} \qquad \text{(II-19)}$$

$$S_{(tg)[i^2;M]} = 40 \text{ dyne-cm/(ma)}^2 \qquad \text{(II-20)}$$

$$S_{(tg)(amp)[e;i^2]} = 0.329 \text{ (ma)}^2\text{/mv} \qquad \text{(II-21)}$$

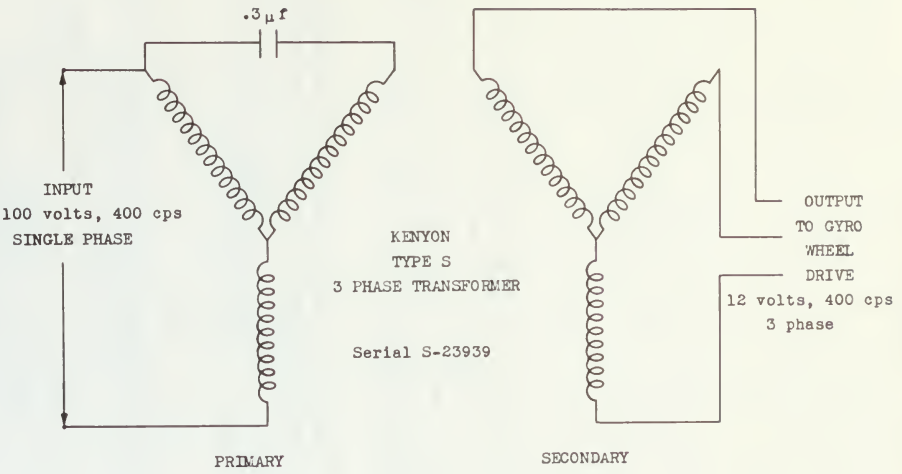

FIG. II-3. NETWORK FOR GYRO DRIVE.

The remaining sensitivities were obtained in the manner described below:

Indicating System Sensitivity:

The single-degree-of-freedom gyro on the rate table was rotated at various angular velocities, and voltage of the signal generator output and prediction angle, P_s, were measured and recorded. Values obtained appear in Table II-1.* From these values Fig. II-4 was plotted, and the slope was measured. From Fig. II-4,

$$S_{i[e;P]} = 118 \text{ mr/volt} \qquad \text{(II-22)}$$

$$S_{i[A;P]} = S_{i[e;P]} S_{(sg)[A;e]} \qquad \text{(II-23)}$$

$$= 118 \times .032$$

$$= 3.77 \text{ mr/mr}$$

The gyro unit used in this study had available 3.5° of travel. With $S_{i[A;P]} = 3.77$, the maximum prediction angle possible is

$$3.77 \times 3.5 = 13.2° \text{ or } 245.5 \text{ mr.}$$

Damping Coefficient:

The damping coefficient of the gyro, C_g, was measured directly by applying known torques and measuring the angular rate output. By this method,

$$C_g = 58.6 \frac{\text{dyne-cm-sec}}{\text{mr}} \qquad \text{(II-24)}$$

Amplifier Sensitivity:

For minimum range of 1200 feet at sea level, for $W_{CL} = 52.36$ mr/sec, from reference (1) the theoretical prediction angle

$$P_{s(corr)} = 19.6 \text{ mr}$$

Since $S_{i[A;P]} = 3.77$, $A_g = \frac{19.6}{3.77} = 5.2$ mr

In steady state, $M_g = S_{(er)[A;M]} A_g$

* See Appendix E for all tables of data from which the sensitivity curves are plotted.

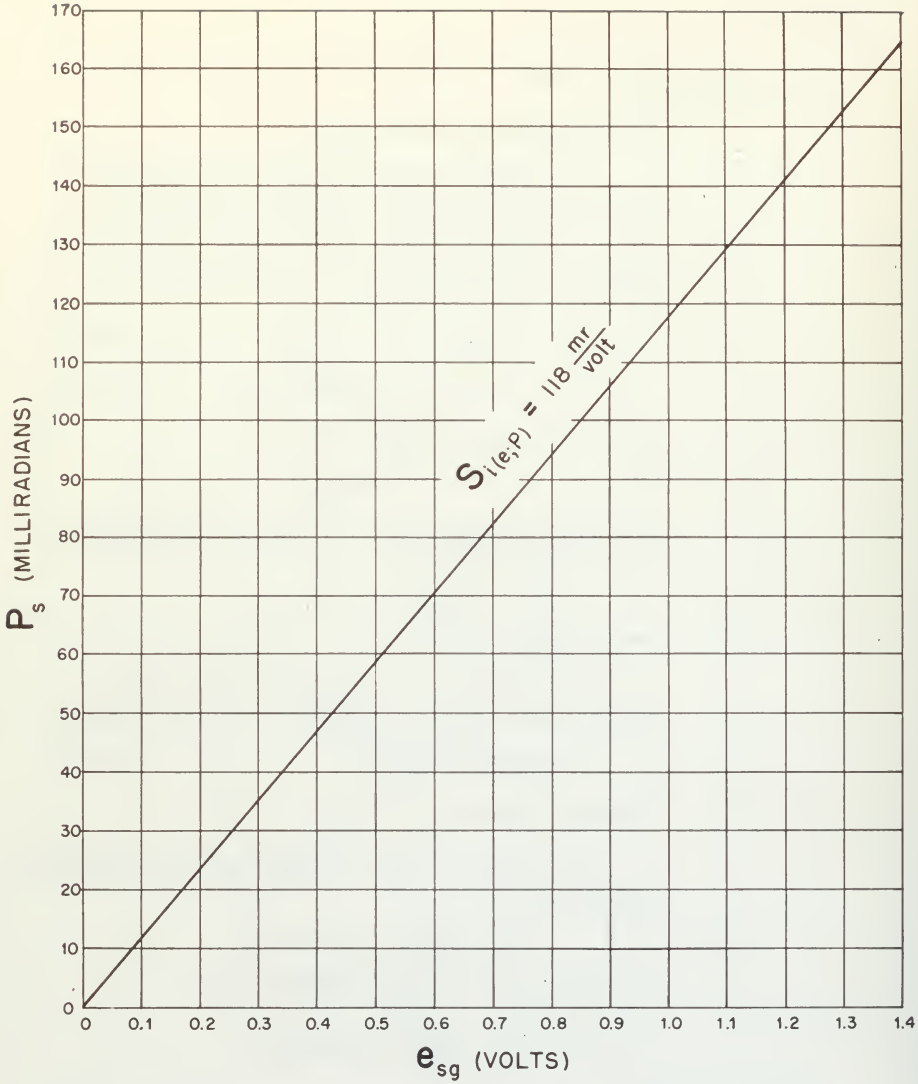

FIG. II-4. DETERMINATION OF $S_{i[e;P]}$ FOR SYSTEM NO. 1.

Since $S_{g[W;M]} = .1 \times 10^6 \frac{\text{dyne-cm-sec}}{\text{radian}} = .1 \times 10^3 \frac{\text{dyne-cm-sec}}{\text{mr}}$,

$$M_g = 52.36 \times .1 \times 10^3$$

$$= 5.236 \times 10^3 \text{ dyne-cm}$$

From (II-5a), using values tabulated above and $S_{R_o[e;e]} = 1.0$, or potentiometer setting all out,

$$S_{(er)[A;M]} = S_{(tg)[i^2;M]} S_{(tg\ amp)[e;i^2]} S_{R_o[e;e]} S_{(amp)[e;e]} S_{(sg)[A;e]}$$

$$= 40 \times .329 \times 1 \times S_{(amp)[e;e]} \times 32$$

$$= 421.12\ S_{(amp)[e;e]}$$

Then

$$S_{(amp)[e;e]} = \frac{5.236 \times 10^3}{421.12 \times 5.2} \qquad \text{(II-25)}$$

$$= 2.39$$

This sensitivity was set by measuring input and output voltages.

5. Prediction Performance of System

When the sensitivities of the components of the system had been determined and/or adjusted, angular rates of the rate table corresponding to W_{CL} were put into the system, and the prediction angles were measured by noting the movement of the reticle image on the inner surface of a section of a sphere of 1 meter radius, located 1 meter from the sight head.

Prediction angle versus W_{CL} at ranges of 1200 feet, 1800 feet and 2400 feet was so obtained. Ranges were changed by using the potentiometer contained in the range box as a voltage divider. The values of prediction angle versus W_{CL} at the various ranges are tabulated in Table II-2, together with $P_{s_{(corr)}}$, as obtained from reference (1). Variations of P_s and $P_{s_{(corr)}}$ with W_{CL} are plotted on Fig. II-5 and variations of P_s and $P_{s_{(corr)}}$ with range are plotted on Fig. II-6. From these figures it may be seen that the accuracy of the system is very good. Higher accuracy could have been obtained

by vibrating the sight head to decrease the effects of coulomb friction in the mirror pivots.

6. Stability Number of System.

From (II-13),

$$(SN) = \left[\frac{(CT)_g}{S_{p[W;P]}} - 1 \right]$$

Substituting for $(CT)_g$ and $S_{p[W;P]}$ with (II-10a) and (II-10b) respectively,

$$(SN) = \left[\frac{\frac{C_g}{S_{(er)[A;M]}}}{\frac{S_{g[W;M]}\, S_{i[A;P]}}{S_{(er)[A;M]}}} - 1 \right]$$

$$= \left[\frac{C_g}{S_{g[W;M]}\, S_{i[A;P]}} - 1 \right] \qquad \text{(II-26)}$$

With the equipment in the laboratory

$$C_g = 0.0586 \times 10^3 \ \frac{\text{dyne-cm-sec}}{\text{mr}} ,$$

$$S_{i[A;P]} = 3.77 \ \frac{\text{mr}}{\text{mr}} , \text{ and}$$

$$S_{g[W;M]} = 0.1 \times 10^3 \ \frac{\text{dyne-cm-sec}}{\text{mr}}$$

Using these values in (II-26),

$$(SN) = \frac{0.0586 \times 10^3}{0.1 \times 10^3 \times 3.77} - 1$$

$$= - 0.845$$

which is unsatisfactory, since for good tracking the (SN) should be 0.2.

For correct prediction, $S_{i[A;P]}$ is fixed at 3.77 mr/mr. $S_{g[W;M]}$ cannot be decreased by more than one-half for satisfactory

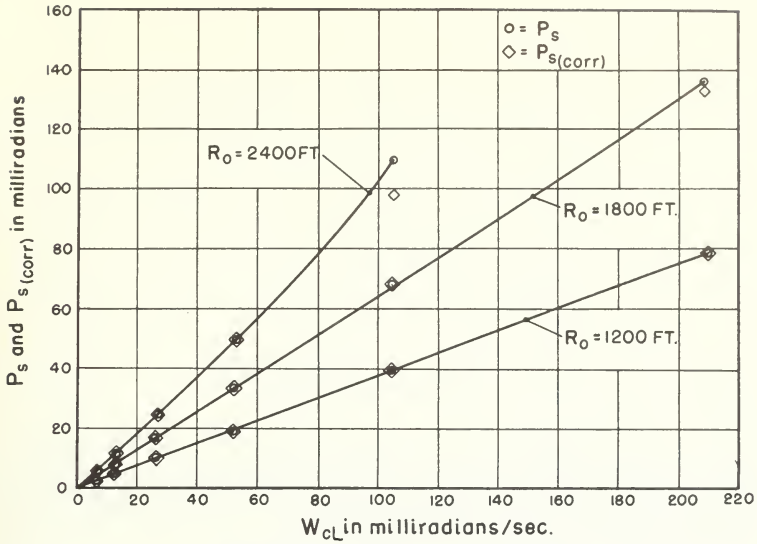

FIG. II-5. P_s vs W_{CL} AT SEA LEVEL

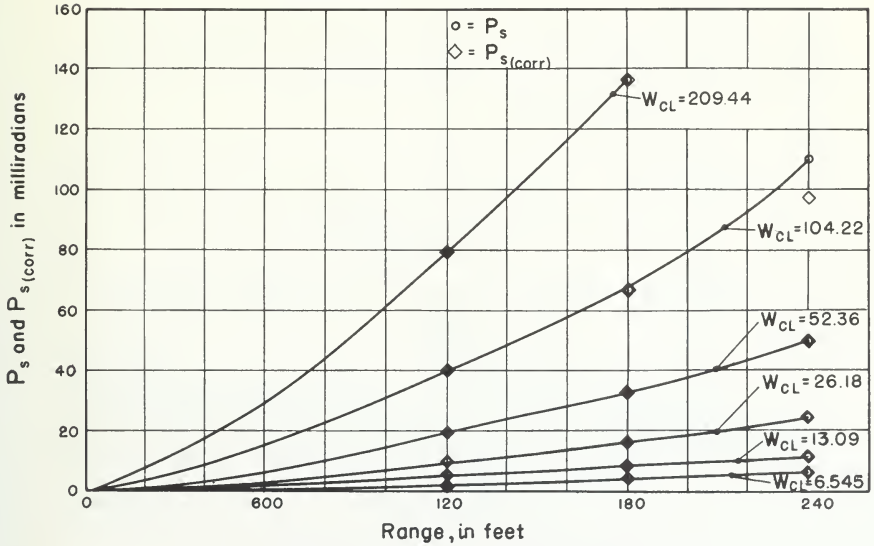

FIG. II-6. P_s vs R_0 AT SEA LEVEL

performance, from Eng. Memo. No. 6411-H-2 (revised).(5).

The value of the remaining quantity, C_g, required for a (SN) of 0.2 for the system is determined below.

$$0.2 = \frac{C_g}{.377 \times 10^3} - 1$$

$$C_g = 1.2 \times .377 \times 10^3$$

$$= .452 \times 10^3 \frac{\text{dyne-cm-sec}}{\text{mr}}$$

A C_g of 0.452×10^3 could not be obtained with the gyro used in the laboratory, because of the temperature-viscosity characteristics of the damping fluid. It could be obtained by use of density 1.0 damping fluid, however, which would entail redesign of the gyro float and container.

7. Tracking Performance of System.

In Paragraph 6 above it has been shown that the system as used in the laboratory was unsatisfactory for tracking, by the (SN) criterion. In addition, it was considered advisable to examine the tracking ratio under both laboratory conditions and the condition with a density 1.0 damping fluid, with

$C_g = 0.452 \times 10^3 \frac{\text{dyne-cm-sec}}{\text{mr}}$.

From (II-17),

$$TR = \frac{1 + [(SN) + 1] S_{p[W;P]} p}{1 + (SN) S_{p[W;P]} p}$$

Using values determined above, for the system in the laboratory,

$$TR = \frac{1 + 0.0582p}{1 - 0.317p} \qquad \text{(II-27)}$$

For the system with (SN) = 0.2, resulting from use of density 1.0 damping fluid,

$$TR = \frac{1 + .45p}{1 + .075p} \qquad \text{(II-28)}$$

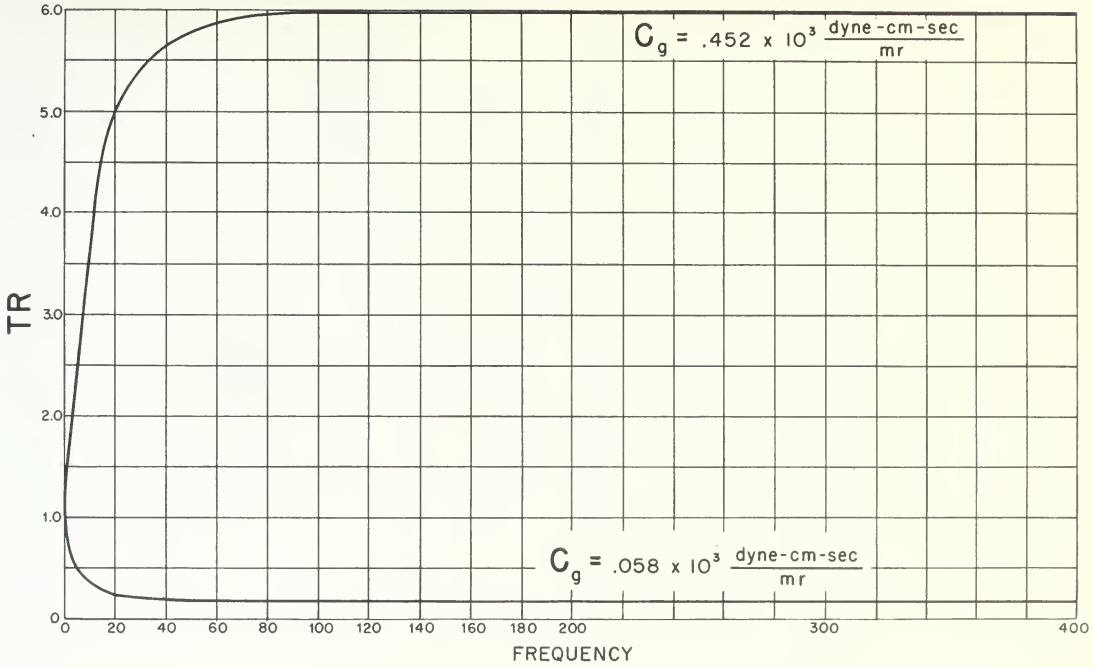

FIG. II-7. TRACKING RATIO Vs TRACKING FREQUENCY, SYSTEM NO 1.

Variation of TR with frequency is tabulated in Table II-3 and is plotted on Fig. II-7. It is evident from Fig. II-7 that the system as used in the laboratory is unsatisfactory for tracking, as noted in paragraph 6 above, and that increasing the C_g to 0.452 x 10^3 dyne-cm-sec/mr will give optimum TR.

8. Conclusions

The performance of the system in computation and in prediction was satisfactory, as is shown on Figs. II-4 and II-5.

The tracking performance of the system as used in the laboratory was unsatisfactory, as is shown in paragraph 7 above and on Fig. II-6, due to insufficient damping in the gyro unit.

Additional damping would make the system satisfactory from both prediction and tracking points of view. The damping coefficient required for satisfactory performance is 0.452 x 10^3 dyne-cm-sec/mr and could not be obtained with the gyro unit which was used. This damping coefficient could be obtained by redesigning the float and case, and using density 1.0 damping fluid.

Since redesign was not possible in the time available for this study, the configuration of System No. 2 was assembled.

CHAPTER III

SYSTEM NO. 2 USING BOTH THE GYRO UNIT AND THE COMPUTER UNIT

1. Introduction

In Chapter II it may be seen that System No. 1, if provided with additional damping, would serve as an adequate replacement for the elevation channel of the A-1 Sight. Since all computation was made on the gyro gimbal shaft, however, the gyro could not be used for stabilization in a fully automatic system.

Accordingly, a configuration using a gyro unit and the separate computer unit which is described in Appendix A was assembled. A functional diagram of that configuration, hereinafter referred to as System No. 2, is shown on Fig. III-1.

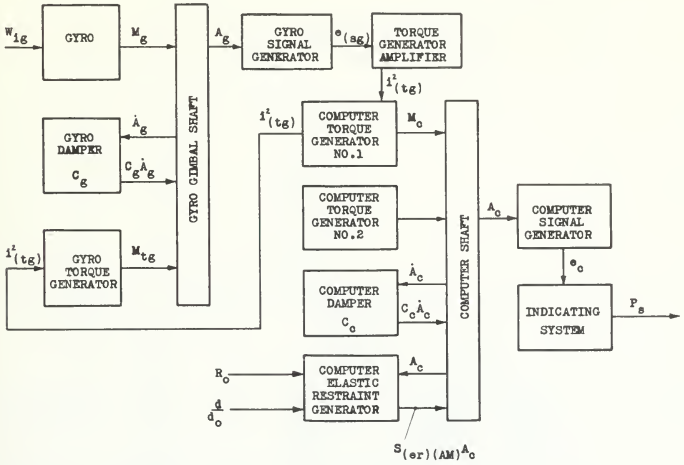

FIG. III-1. FUNCTIONAL DIAGRAM OF SYSTEM NO. 2.

A fully automatic system utilizing System No. 2 as a component appears as Fig. III-2. One requirement of any such system is that it permit manual tracking, as well as function automatically. The following analysis of System No. 2 is predicated on manual tracking.

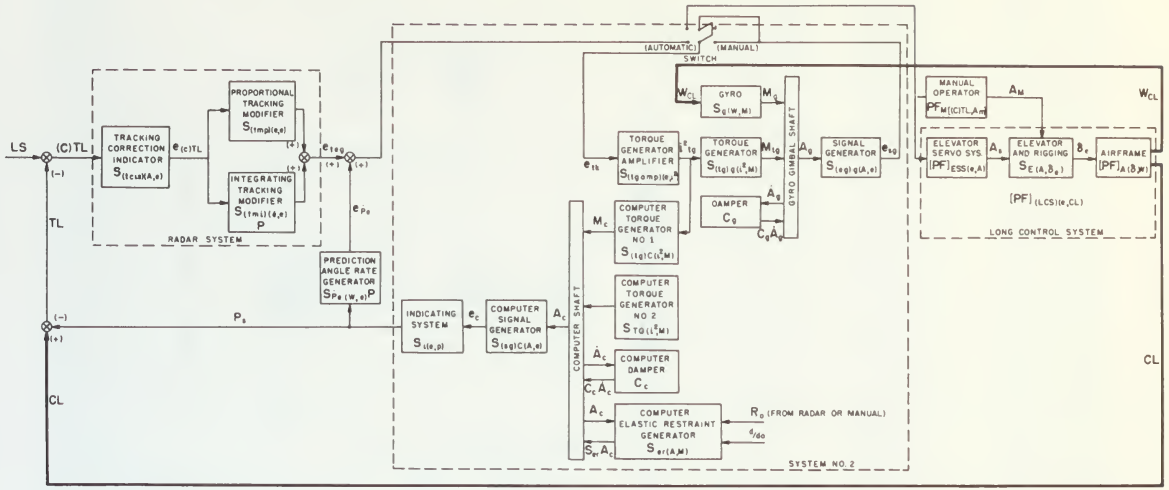

FIG III-2. FUNCTIONAL DIAGRAM OF AN AUTOMATIC TRACKING SYSTEM UTILIZING SYSTEM NO. 2.

2. Equations of the System.

For System No. 2, as shown in Fig. III-1, the basic equations are:

$$W_{(CL)} S_{g(W;M)} = C_g \dot{A}_g + S_{(tg)g(i^2;M)} i^2_{(tg)} \quad \text{(III-1)}$$

$$e_{(sg)} = S_{(sg)(A;e)} A_g \quad \text{(III-2)}$$

$$i^2_{(tg)} = S_{(tg\ amp)(e;i^2)} e_{(sg)g} \quad \text{(III-3)}$$

$$M_c = S_{(tg)\,c\,(i^2;M)} i^2_{(tg)} \quad \text{(III-4)}$$

$$M_c = S_{(er)\,c\,(A,i^2;M)} i^2_{(er)} A_c + C_c \dot{A}_c \quad \text{or} \quad \text{(III-5)}$$

$$M_c = S_{(er)\,c\,(A;M)} A_c + C_c \dot{A}_c$$

$$e_c = S_{(sg)\,c\,(A;e)} A_c \quad \text{(III-6)}$$

$$P_s = S_{i(A;P)} A_c \quad \text{or} \quad A_c = \frac{P_s}{S_{i(A;P)}} \quad \text{(III-7)}$$

differentiating equation (III-7) gives,

$$\dot{P}_s = S_{i(A;P)} \dot{A}_c \quad \text{or} \quad \dot{A}_c = \frac{\dot{P}_s}{S_{i\,(A;P)}} \quad \text{(III-8)}$$

Equations (III-4), (III-7) and (III-8) in (III-5) gives,

$$\frac{C_c}{S_{(er)\,c\,(A;M)}} \dot{P}_s + P_s = \frac{S_{i(A;P)}\, S_{(tg)\,c\,(i^2;M)}}{S_{(er)\,c\,(A;M)}} i^2_{(tg)} \quad \text{(III-9)}$$

Define:

$$(CT)_c \triangleq \frac{C_c}{S_{(er)(A;M)}} \tag{III-10}$$

$$[SR]_{(i^2;P)} = \frac{S_{i(A;P)}\, S_{(tg)\,c\,(i^2;M)}}{S_{(er)(A;M)}} \tag{III-11}$$

Then equation (III-9) becomes,

$$(CT)_c \dot{P}_S + P_S = [SR]_{(i^2;P)}\, i^2_{(tg)} \tag{III-12}$$

from which,

$$P_S = \frac{[SR]_{(i^2;P)}\, i^2_{(tg)}}{[(CT)_c\, p + 1]} \tag{III-13}$$

Equations (III-2) and (III-3) in (III-1) gives,

$$\frac{C_g}{S_{(tg)g(i^2;M)}\, S_{(tg\ amp)(e;i^2)}\, S_{(sg)g(A;e)}} \dot{A}_g + A_g$$

$$= \frac{S_{g(W;M)}}{S_{(tg)g(i^2;M)}\, S_{(tg\ amp)(e;i^2)}} \frac{W_{(CL)}}{S_{(sg)g(A;e)}} \tag{III-14}$$

Define:

$$(CT)_g = \frac{C_g}{S_{(tg)g(i^2;M)}\, S_{(tg\ amp)(e;i^2)}\, S_{(sg)g(A;e)}} \qquad \text{(III-15)}$$

$$[SR]_{(W,A)} = \frac{S_{g(W,M)}}{S_{(tg)g(i^2;M)}\, S_{(tg\ amp)(e;i^2)}\, S_{(sg)g(A;e)}} \qquad \text{(III-16)}$$

Then equation (III-14) becomes,

$$(CT)_g \dot{A}_g + A_g = [SR]_{(W;A)}\, W_{(CL)} \qquad \text{(III-17)}$$

from which,

$$A_g = \frac{[SR]_{(W;A)}}{[(CT)_g\, p + 1]}\, W_{(CL)} \qquad \text{(III-18)}$$

Equations (III-18) and (III-3) in (III-2) gives,

$$i^2_{(tg)} = \frac{[SR]_{(W;i^2)}}{[(CT)_g\, p + 1]}\, W_{(CL)} \qquad \text{(III-19)}$$

where

$$[SR]_{(W;i^2)} = \frac{S_{g(W;M)}}{S_{(tg)g(i^2;M)}}$$

Equation (III-19) into (III-13) gives,

$$P_s = \frac{[SR]_{(i^2;P)}\, [SR]_{(W;i^2)}}{[(CT)_g\, p + 1]\, [(CT)_c\, p + 1]}\, W_{(CL)} \qquad \text{or} \qquad \text{(III-20)}$$

or

$$\frac{P_s}{W_{(CL)}} = \frac{S_{p(W;P)}}{[(CT)_g\, p + 1]\,[(CT)_c\, p + 1]} \tag{III-21}$$

For tracking considerations:

$$CL = TL + P_s \tag{III-22}$$

Differentiating equation (III-22)

$$W_{(CL)} = W_{(TL)} + \dot{P}_s \tag{III-23}$$

Equation (III-23) in (III-21) gives,

$$P_s = \frac{S_{p(W;P)}\,[W_{(TL)} + \dot{P}_s\,]}{[(CT)_g\, p + 1]\,[(CT)_c\, p + 1]} \tag{III-24}$$

from which,

$$\frac{P_s}{W_{(TL)}} = \frac{S_{p(W;P)}}{1 + [(CT)_g + (CT)_c - S_{p(W;P)}]\, p + (CT)_g\,(CT)_c\, p^2} \tag{III-25}$$

$$(TR) = \frac{CL}{TL} = \frac{W_{(CL)}}{W_{(TL)}} = \frac{W_{(CL)}}{P_s}\,\frac{P_s}{W_{(TL)}} \tag{III-26}$$

Equations (III-21) and (III-25) in (III-26) gives,

$$\frac{W_{(CL)}}{W_{(TL)}} = \frac{CL}{TL} = \frac{1 + [(CT)_g + (CT)_c]\, p + (CT)_g\,(CT)_c\, p^2}{1 + [(CT)_g + (CT)_c - S_{p(W;P)}]\, p + (CT)_g\,(CT)_c\, p^2} \tag{III-27}$$

3. Description of Laboratory Setup.

The power pack, described in Chapter II, was used for driving the gyro wheel, for supplying reference voltages and for exciting the signal generators.

The output of the gyro signal generator was fed into the torque generator amplifier, the output of which energized the first torque generator on the computer in series with the torque generator on the gyro unit.

Range input was obtained from a 300 volt B+ supply, and was set by means of a potentiometer in series with the elastic restraint generator of the computer.

The output from the computer signal generator, a voltage proportional to prediction angle, was fed into the servo amplifier of the A-1 Sight.

Phasing of the reference voltage for the servo amplifier with the sight head signal generator output voltage was accomplished in the same manner as described in Chapter II.

As in System No. 1, altitude correction was a modification of range input. In the laboratory, this modification was accomplished by a change in the range potentiometer setting. Curvature correction, had it been taken into account, could have been made utilizing the second torque generator of the computer unit.

4. Determination and Adjustment of System Sensitivities.

The various component sensitivities shown in equations (III-1) through (III-27) were taken from Appendix A or were measured directly from the physical equipment of the laboratory setup. The damping coefficients of the gyro unit and the computer unit were measured by putting known torques into the units and measuring the angular rate output. By this method, C_g was found to be 58.6 dyne-cm-sec/mr and C_c to be 130 dyne-cm-sec/mr.

The sensitivity of the indicating system for voltage in, prediction angle out was measured directly by noting the angular displacement of the light spot, P_s, for various input voltages to the sight head servo amplifier. These measurements are shown in Table III-1 and Fig. III-3.

A tabulation of sensitivities, coefficients, and characteristic times used in this analysis are shown in Table III-2.

The range and altitude function inputs were added to the system by varying the excitation current to the elastic restraint generator by means of a potentiometer in the 300 volt d.c. supply line. The amount of excitation current necessary for the proper range and altitude is given in Tables III-6 and III-7.

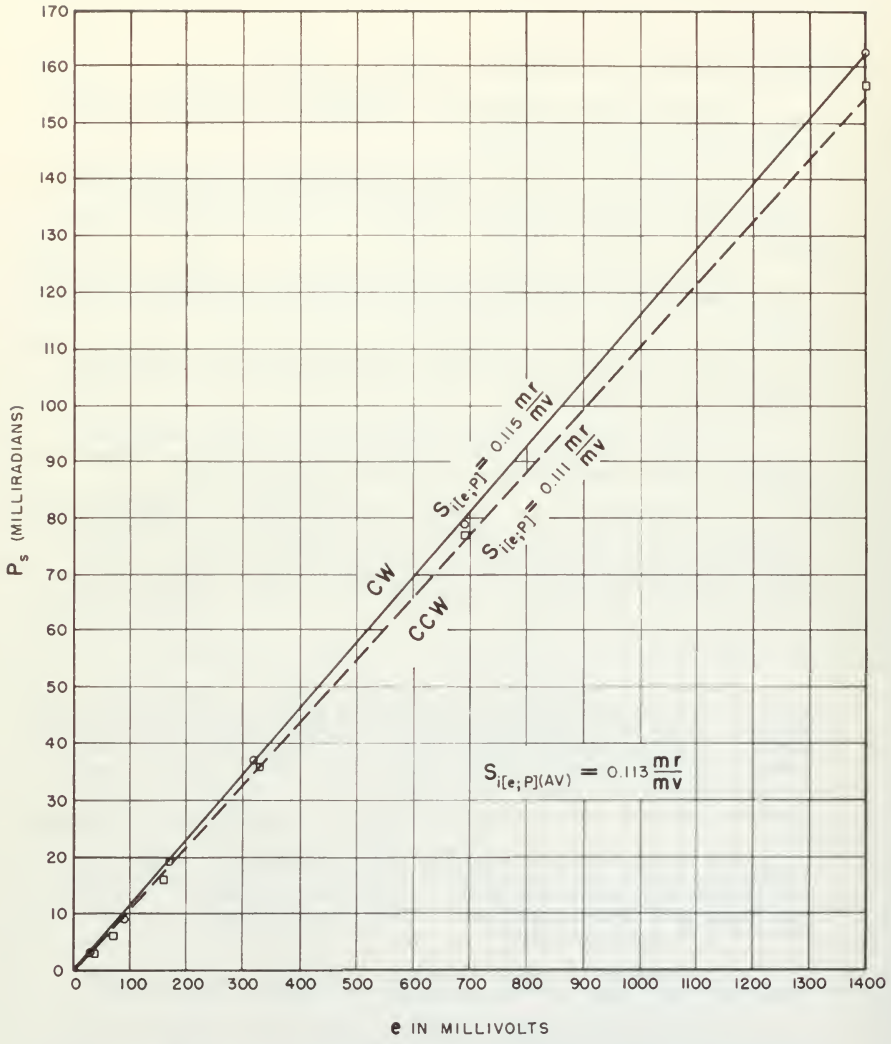

FIG. III-3. DETERMINATION OF $S_{i[e;P]}$

5. Prediction Performance of the System.

It can be seen from equation

$$\frac{P_s}{W_{(CL)}} = \frac{S_{p(W;P)}}{[(CT)_g\, p + 1]\,[(CT)_c\, p + 1]}, \qquad \text{(III-21)}$$

that from the standpoint of generating the proper prediction angle for various angular rate inputs, the system can never become unstable.

Using values shown in Table III-1, the amplitude ratio and phase angle of equation (III-21) were plotted versus angular frequency for three different ranges at sea level. For these plots which verify the stability of the prediction system, see Figs. III-4 and III-5.

Experimental data was also taken for prediction angle versus input angular rates for various ranges both at sea level and 16,000 feet. These data are shown in tabular form in Tables III-6 and III-7, and are plotted in Figs. III-6 and III-7. From Figs. III-6 and III-7, cross plots were made of $S_{p(W;P)}$ versus R_o. These cross plots are shown in Figs. III-8 and III-9. The experimental curves of Figs. III-8 and III-9 are compared with the theoretical curves and appear to agree very well, showing that the system behaves satisfactorily in prediction.

6. Performance of the System for Manual Tracking.

It can be seen upon examination of equation

$$\frac{CL}{TL} = \frac{1 + [(CT)_g + (CT)_c]\, p + (CT)_g\,(CT)_c\, p^2}{1 + [(CT)_g + (CT)_c - S_{p(W;P)}]\, p + (CT)_g\,(CT)_c\, p^2}, \qquad \text{(III-27)}$$

that the system will be unstable in tracking when $S_{p_{(W;P)}} > [(CT)_g + (CT)_c]$. Therefore, it appears logical to establish tracking stability criteria by defining a "damping-ratio ratio" such that,

$$(DRR) = \frac{[(CT)_g + (CT)_c - S_{p(W;P)}]}{[(CT)_g + (CT)_c]} \qquad \text{(III-28)}$$

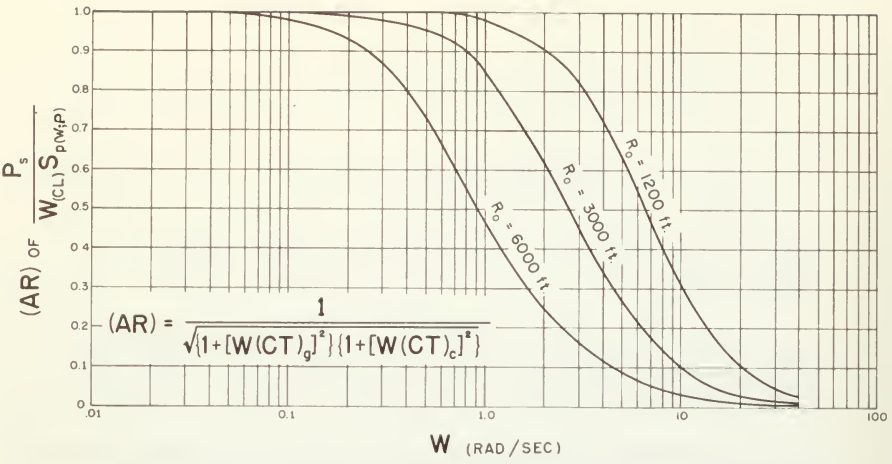

FIG. III-4. (AR) OF $\frac{P_s}{W_{(CL)}S_{p(W;P)}}$ Vs. W AT SEA LEVEL.

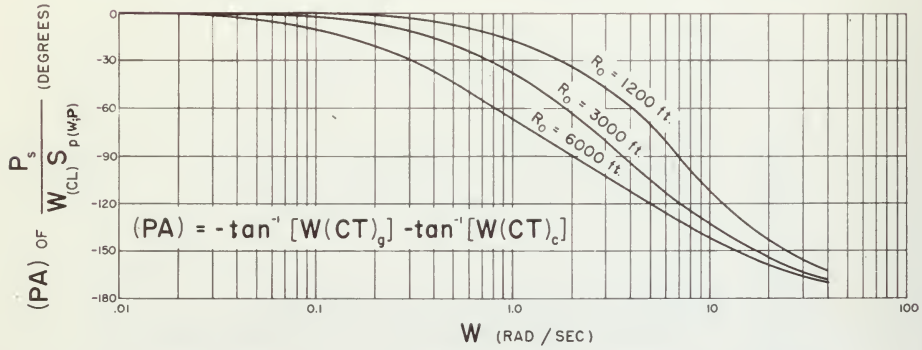

FIG. III-5. (PA) OF $\frac{P_s}{W_{(CL)}S_{p(W;P)}}$ Vs W AT SEA LEVEL.

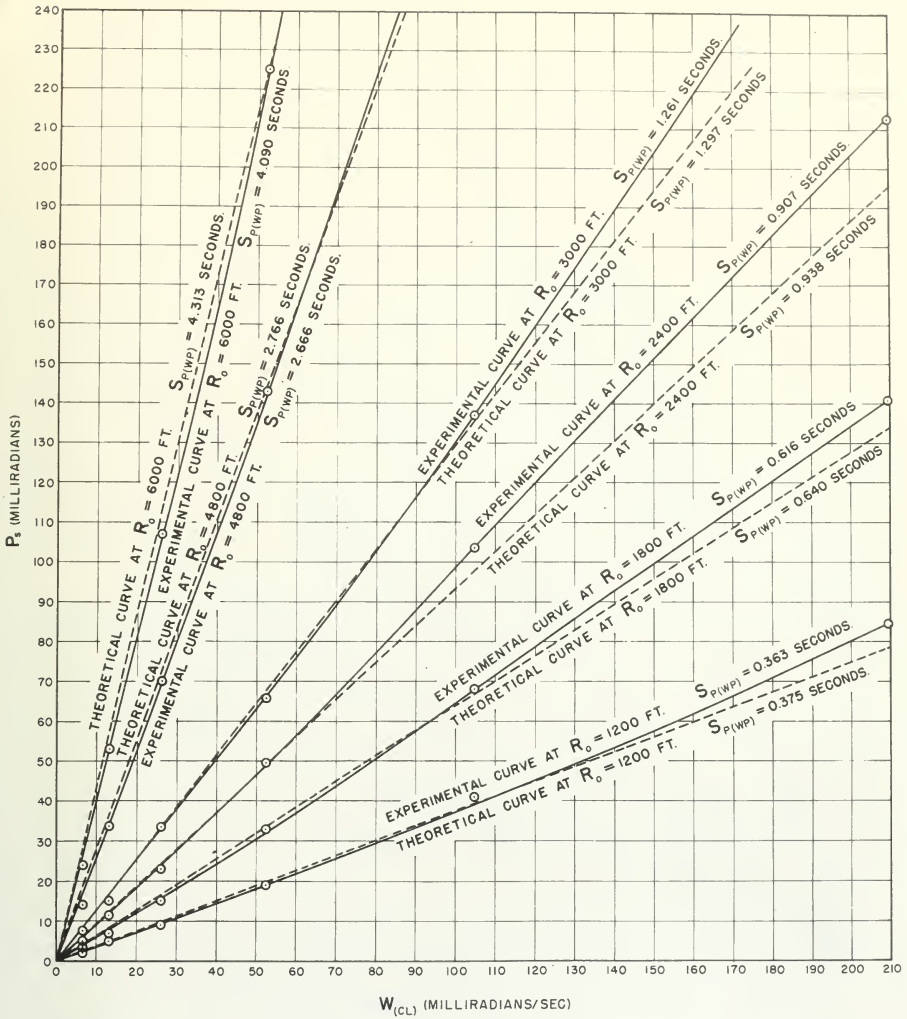

FIG. III-6. EXPERIMENTAL AND THEORETICAL PREDICTION ANGLE VS. INPUT ANGULAR VELOCITY FOR VARIOUS RANGES AT SEA LEVEL, SYSTEM NO. 2.

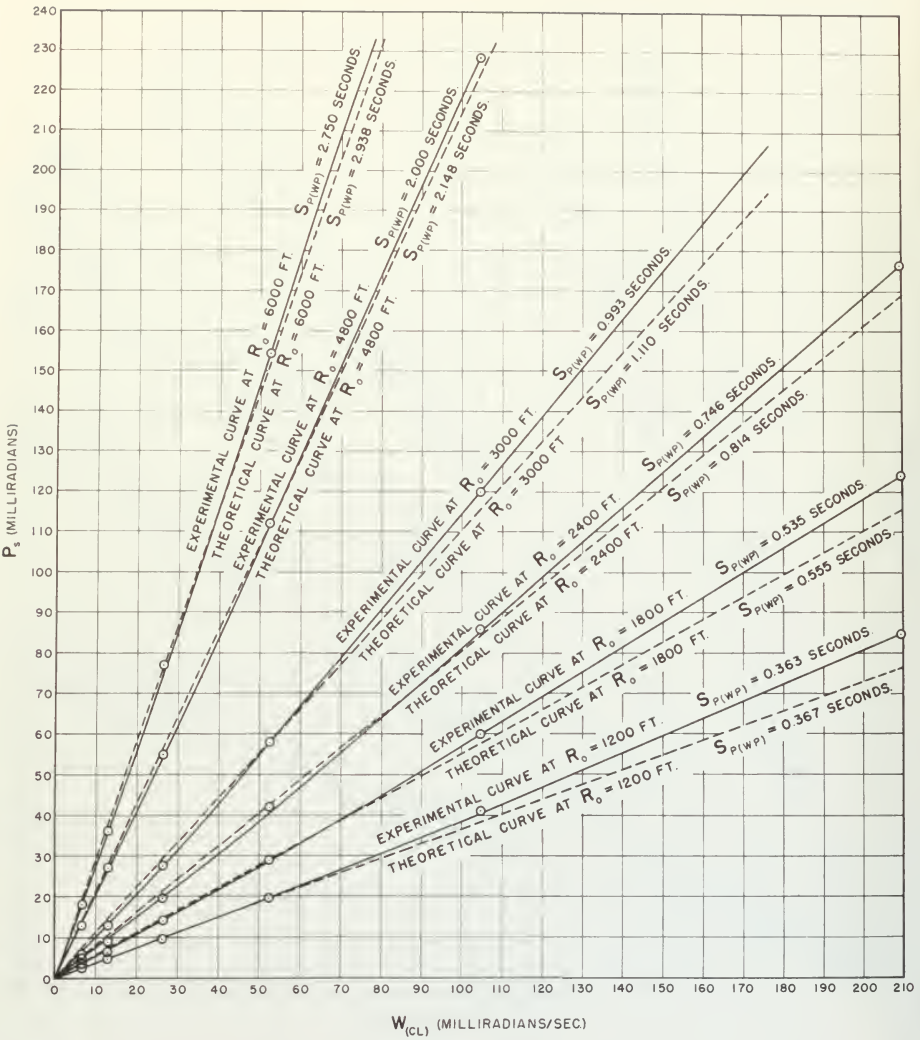

FIG. III-7. EXPERIMENTAL AND THEORETICAL PREDICTION ANGLE VS. INPUT ANGULAR VELOCITY FOR VARIOUS RANGES AT 16,000 FT., SYSTEM NO. 2.

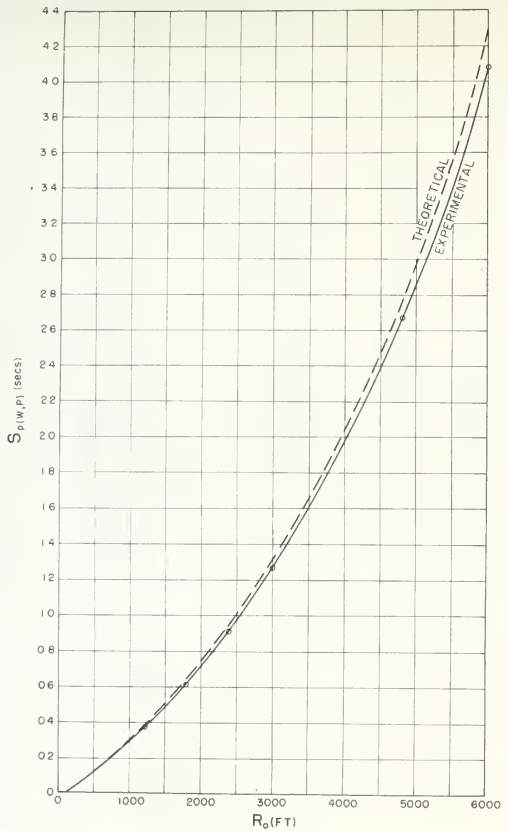

FIG. III-8. $S_{p(W;P)}$ vs R_o AT SEA LEVEL, SYSTEM NO. 2.

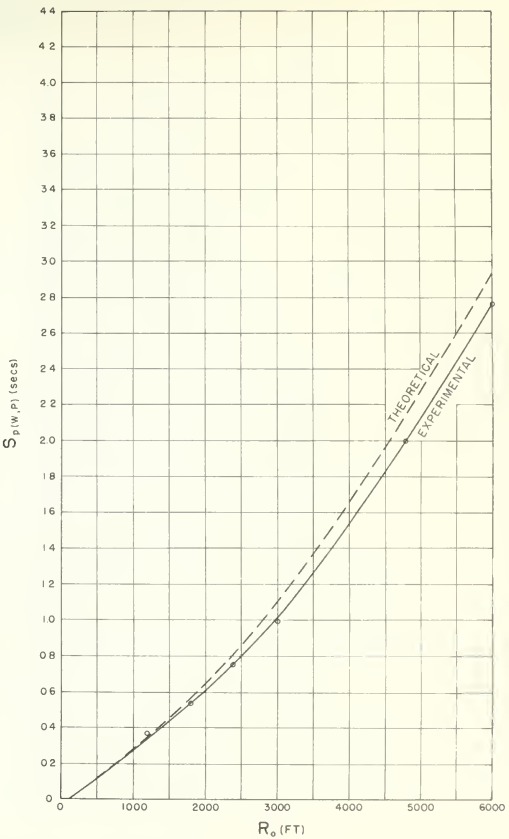

FIG. III-9. $S_{p(W;P)}$ vs R_o AT 16,000 FT., SYSTEM NO. 2.

or

$$(DRR) = \left[1 - \frac{S_{p(W;P)}}{[(CT)_g + (CT)_c]} \right] \qquad \text{(III-28a)}$$

Then if (DRR) ≤ 0, the system is unstable for tracking, but if (DRR) > 0, the system is stable for tracking. In the light of this criteria, equation (III-27) indicates that the tracking system is unstable at all but the lowest range. The stability criteria are also substantiated by Fig. III-10 in which (DRR) is plotted versus range. It is noted that (DRR) becomes negative at a range of approximately 860 feet, and therefore the system becomes unstable in tracking at this point. These stability criteria are further substantiated by tests made on the Philbrick electronic simulator as described in the next sub-section of this Chapter.

As a remedy for the tracking instability shown above, let a (DRR) of + 0.1 at a range of 6000 feet be required. This requirement would necessitate a gyro characteristic time of 2.9 seconds and a consequent gyro damping coefficient of 1220 dyne-cm-sec/mr or roughly twenty times the present C_g. Such a C_g is obviously impossible to obtain with the density 2.0 damping fluid presently in use in the gyro unit, and could only be realized by use of density 1.0 damping fluid plus an extensive redesign of the gyro float and case.

However, if the damping coefficient of the computer, C_c, were increased so that,

$$C_c = S_{p(W;P)} = \frac{1190}{i^2_{(er)}} \text{ seconds, then}$$

$$(DRR) = \left[1 - \frac{\frac{1190}{i^2_{(er)}}}{(CT)_g + \frac{1190}{i^2_{(er)}}} \right] \qquad \text{(III-29)}$$

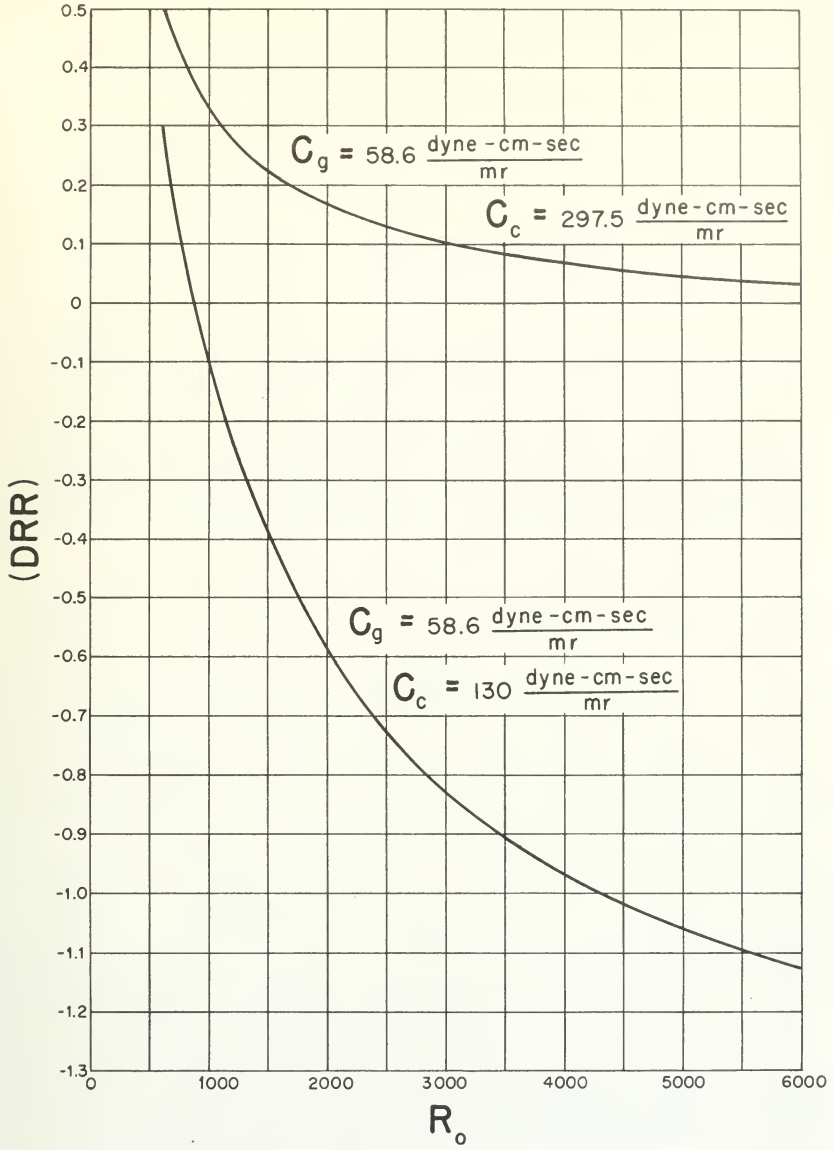

FIG. III-10. (DRR) Vs R_o AT SEA LEVEL FOR VARIOUS DAMPING COEFFICIENTS. SYSTEM NO. 2.

If such is the case, it is seen from Table III-10 and Fig. III-10 that (DRR) is always positive, and therefore the system will be stable in tracking at all ranges. In order that $(CT)_c = S_{p(W;P)}$, C_c must be increased from 130 dyne-cm-sec/mr to 297.5 dyne-cm-sec/mr. This might be accomplished by reducing the stabilization temperature of the computer unit, but it is more likely that density 1.0 fluid plus redesign of the computer unit will be required.

Another method for obtaining tracking stability would consist of the insertion of a lead network into the system which would exactly cancel the lag term introduced by the gyro unit. Such a procedure would result in a return to a first-order, "ideal" system for which a stability number could be defined. However, insertion of the lead network would permit some undesirable, high frequency noise to leak into the system,so some sort of filter circuit must be provided to eliminate such effects. Also, a large increase in computer damping must be realized for such a system to be stable in tracking, an increase only obtainable by redesign of the computer unit and the use of density 1.0 damping fluid.

The equations for the resulting first-order system are:

$$(SN)\, S_{p(W,P)}\, \dot{P}_S + P_S = S_{p(W,P)}\, W_{(TL)} \qquad \text{(III-30)}$$

where (SN) is defined as,

$$(SN) = \left[\frac{(CT)_c}{S_{p(W,P)}} - 1 \right] \qquad \text{(III-31)}$$

but since

$$W_{(CL)} = W_{(TL)} + \dot{P}_S \qquad \text{(III-23)}$$

then

$$\frac{W_{(CL)}}{W_{(TL)}} = \frac{(SN + 1)\, S_{p(W,P)}\, p + 1}{(SN)\, S_{p(W,P)}\, p + 1} \qquad \text{(III-32)}$$

Then for system stability, it is seen that the control line must lead the tracking line so the stability number, (SN), must be greater than zero. If such is the case, it can be seen from equation (III-31) that $(CT)_c$ must be greater than $S_{p(W;P)}$ in order to have stability in tracking.

However, since the (SN) of the system as it stands now is -0.56; to obtain an (SN) of + 0.2 and a stable tracking system, a C_c of 357 dyne-cm-sec/mr would be required, meaning again a redesign of the computer unit and a shift to density 1.0 damping fluid.

If a step input in $W_{(TL)}$ is put into the system, then;

$$W_{(CL)}(p) = \frac{(SN + 1) S_{p(W,P)} p + 1}{p [(SN) S_{p(W,P)} p + 1]} \qquad \text{(III-33)}$$

from which the transient response, $W_{(CL)}(t)$, is,

$$W_{(CL)}(t) = [1 + \frac{1}{(SN)} e^{- \frac{t}{(SN) S_{p(W,P)}}}] \qquad \text{(III-34)}$$

Then at $t = 0$

$$W_{(CL)}(t) = 1 + \frac{1}{(SN)} \qquad \text{(III-35)}$$

From equations (III-34) and (III-35), it can be seen that for a step input in $W_{(TL)}$ at positive values of stability number, the response, $W_{(CL)}$, jumps immediately to a peak leading $W_{(TL)}$, gradually decaying exponentially to the step function in $W_{(TL)}$. Thus it is seen that $W_{(CL)}$ leads $W_{(TL)}$ at all times as it should for stable tracking. This stability is substantiated in the next sub-section of this Chapter.

7. Simulated Performance of System No. 2 in Tracking.

In order to substantiate the stability criteria in tracking established in the preceding sub-section, the tracking problem for System No. 2, both for the "ideal" case and for the case using the gyro unit and the computer, was set up on the Philbrick Electronic Simulator at the Instrumentation Laboratory, Massachusetts Institute of Technology. A discussion of the results obtained follows.

The equation for the ideal case, (III-32), was mechanized as shown in Fig. III-11 using an add box, an integration box and two coefficient boxes. A step input in $W_{(TL)}$ was then put into the system, and the transient response, $W_{(CL)}(t)$, for various values of stability number was viewed by means of a cathode ray oscilloscope. Photographs of the input and output of this system are shown in Figs. III-13 through III-17. It can be seen from these photographs that for a step input in $W_{(TL)}$, the response leads the input quantity for all positive values of (SN); and therefore the system is stable in tracking. It can also be noted $[W_{(CL)}]_o = [1 + \frac{1}{(SN)}]$ in each case, a fact established mathematically in the preceding sub-section. For (SN) = 0 and for negative values of (SN), it was observed that the system was definitely unstable.

The equation for the system using both the gyro unit and the computer, (III-27), was mechanized as shown in Fig. III-12 using two lag boxes, a coefficient box, a derivative box and an add box. A step input in $W_{(TL)}$ was then put into the system, and the transient response, $W_{(CL)}(t)$, for various conditions was viewed by means of the cathode ray oscilloscope. Photographs of the input and output for this system are shown in Figures III-18 through III-30.

Figure III-18 shows the system response for a step input in $W_{(TL)}$ at a range of 600 feet using system coefficients and sensitivities established in Table III-2. Although there are some second order oscillations present in the response curve due mainly to insufficient damping in the gyro unit, it is considered that the system is stable at this range as predicted in the preceding sub-section, since the control line leads the tracking line initially, and then oscillates about the tracking line before settling down to its steady state value. Figure III-19 shows the system response at a range of 850 feet just before becoming unstable. This instability was also predicted by the (DRR) stability criteria in sub-section 6.

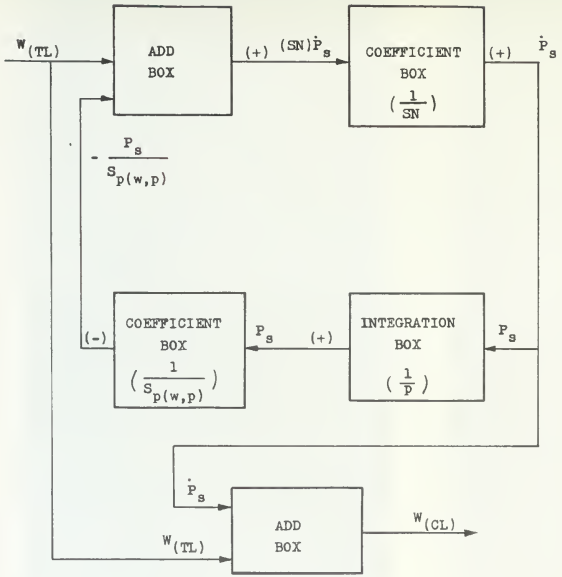

EQUATION (III-32) $\frac{W_{(CL)}}{W_{(TL)}} = \frac{(SN+1)S_{p(w,p)}^{p+1}}{(SN)S_{p(w,p)}^{p+1}}$

FIG. III-11. MECHANIZATION OF FIRST ORDER SYSTEM NO. 2.

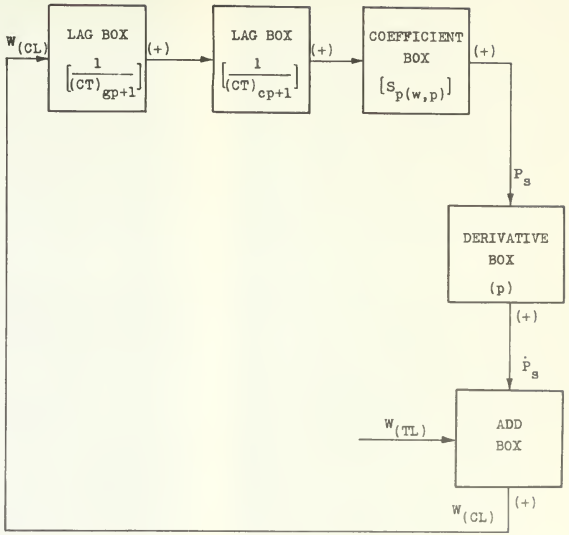

EQUATION (III-27) $\frac{W_{(CL)}}{W_{(TL)}} = \frac{1+[(CT)_g+(CT)_c]p+(CT)_g(CT)_c p^2}{1+[(CT)_g+(CT)_c-S_{p(w,p)}]p+(CT)_g(CT)_c p^2}$

FIG. III-12. MECHANIZATION OF SECOND ORDER SYSTEM NO. 2.

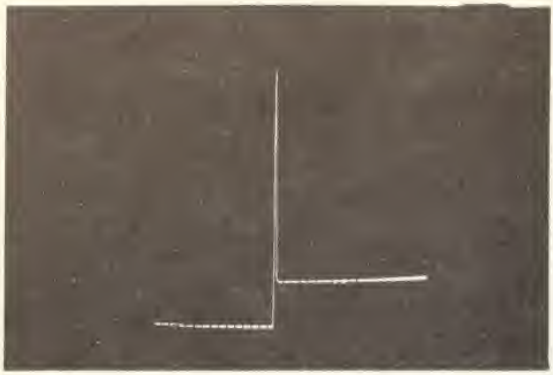

FIG. III-13
$W_{(CL)}$ RESPONSE TO STEP IN $W_{(TL)}$ FOR FIRST ORDER SYSTEM NO. 2, (SN) = 0.2 ; $S_{P(W, P)}$ = 0.375 SEC.

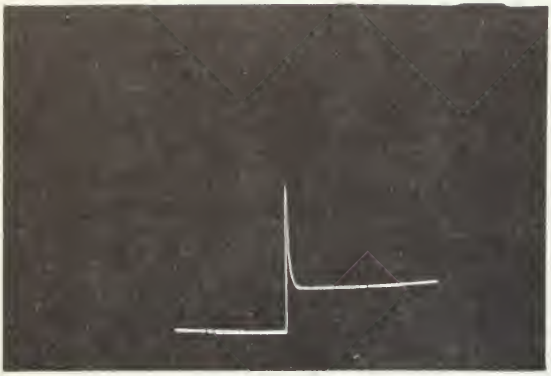

FIG. III-14
$W_{(CL)}$ RESPONSE TO STEP IN $W_{(TL)}$ FOR FIRST ORDER SYSTEM NO. 2, (SN) = 0.4 ; $S_{P(W, P)}$ = 0.375 SEC.

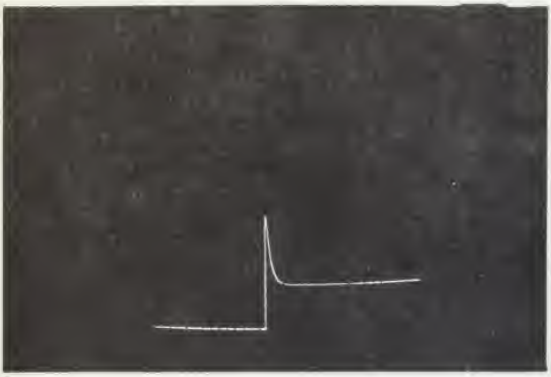

FIG. III-15
$W_{(CL)}$ RESPONSE TO STEP IN $W_{(TL)}$ FOR FIRST ORDER SYSTEM NO. 2, (SN) = 0.6 ; $S_{P(W, P)}$ = 0.375 SEC.

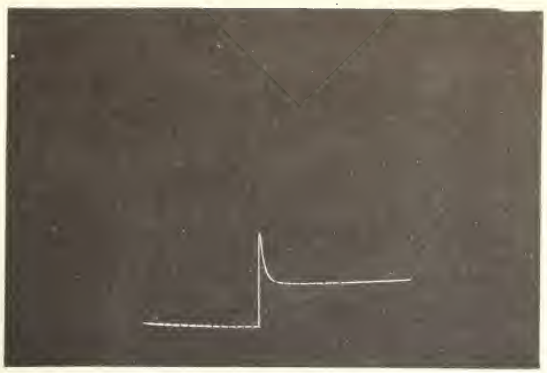

FIG. III-16
$W_{(CL)}$ RESPONSE TO STEP IN $W_{(TL)}$ FOR FIRST ORDER SYSTEM NO. 2, (SN) = 0.8; $S_{P(W,P)}$ = 0.375 SEC.

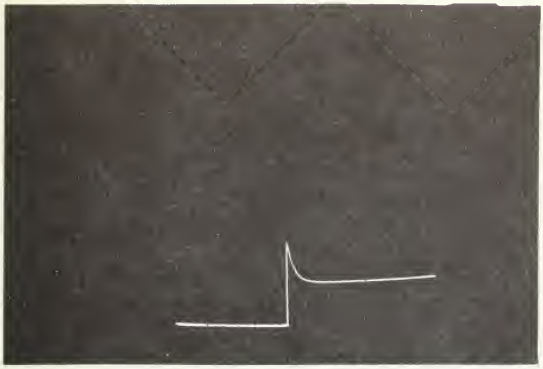

FIG. III-17
$W_{(CL)}$ RESPONSE TO STEP IN $W_{(TL)}$ FOR FIRST ORDER SYSTEM NO. 2, (SN) = 1.0 ; $S_{P(W,P)}$ = 0.375 SEC.

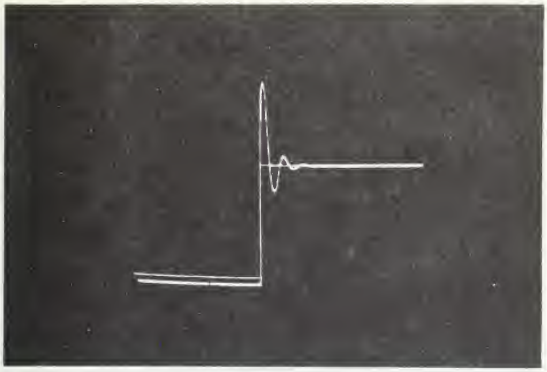

FIG. III-18
$W_{(CL)}$ RESPONSE TO STEP IN $W_{(TL)}$ FOR SECOND ORDER SYSTEM NO. 2,
R_o = 600 FT. ;
$(CT)_g$ = 0.14 SEC.;
$(CT)_c$ = 0.0612 SEC.;
$S_{P(W,P)}$ = 0.14 SEC.

Figures III-20 through III-22 show the effect on the system response of increasing the characteristic time of the computer until it is equal to $S_{p(W;P)}$ holding $(CT)_g$ constant at 0.14 seconds as before. This procedure, in effect, increases the damping of the computer to 297.5 dyne-cm-secs/mr as previously discussed. Upon examination of Figs. III-20 through III-22, it is noted that as the range is increased, the amplitude of the second order oscillations is also increased, meaning that the (DRR) is approaching zero as shown in Fig. III-10. Then it can be seen that the system is stable in tracking at all practical ranges but approaches instability as the range increases.

Figures III-23 through III-25 show the effect of holding $(CT)_c = S_{p(W;P)}$ and increasing the damping of the gyro unit so that the gyro characteristic time is increased to 0.70 seconds. It can be noted that the increase in the amplitude of the second order oscillation, as range is increased, is not so pronounced as in the previous case, indicating that the (DRR) is not approaching as close to zero for the same range in both cases. This fact can be verified by examing the (DRR) equation,

$$(DRR) = 1 - \left[\frac{S_{p(W;P)}}{(CT)_g + (CT)_c}\right] \qquad \text{(III-28a)}$$

where $S_{p(W;P)} = (CT)_c$ for both cases, and $(CT)_{g1} < (CT)_{g2}$.

Figures III-26 through III-30 show the effect of increasing the gyro damping so that $(CT)_g$ increases accordingly to 0.70 seconds, while allowing $(CT)_c$ and $S_{p(W;P)}$ to vary in the manner shown in Table III-2. Thus it is shown that by increasing the gyro damping coefficient to five times its original value, the range at which system instability occurs is increased. In this case the (DRR) becomes zero and consequent system instability occurs at a range of approximately 2700 feet. It was shown in sub-section 6 that to insure a (DRR) of + 0.1 at a range of 6000 feet, thereby realizing stability in tracking for the system throughout the practical range of the A-1 Sight, an increase in the gyro damping coefficient to approximately twenty times its original value would be required.

Figure III-30 is given here to show the transient response output of prediction angle for a step input in $W_{(TL)}$, and to show that it also has a stable response at a range of 600 feet, using the coefficients and sensitivities shown in Table III-2.

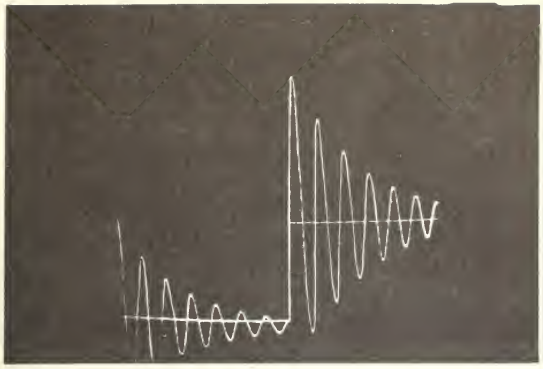

FIG. III-19
$W_{(CL)}$ RESPONSE TO STEP IN $W_{(TL)}$ FOR SECOND ORDER SYSTEM NO. 2,
R_o = 850 FT.;
$(CT)_g$ = 0.14 SEC.;
$(CT)_c$ = 0.106 SEC.;
$S_{P(W,P)}$ = 0.251 SEC.

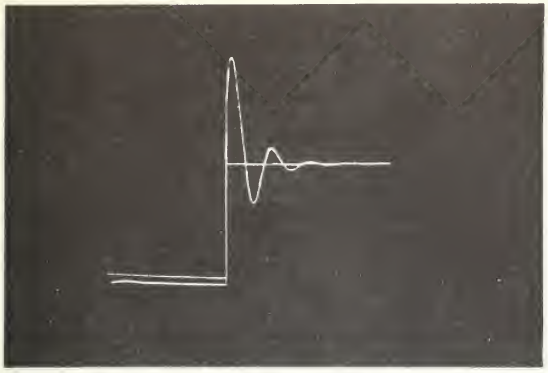

FIG. III-20
$W_{(CL)}$ RESPONSE TO STEP IN $W_{(TL)}$ FOR SECOND ORDER SYSTEM NO. 2,
R_o = 1200 FT.;
$(CT)_g$ = 0.14 SEC.;
$(CT)_c$ = $S_{P(W,P)}$ = 0.275 SEC.

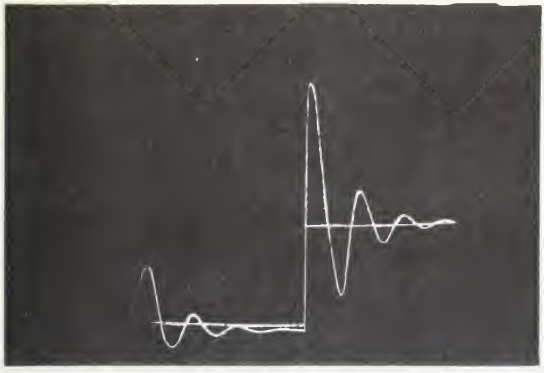

FIG. III-21
$W_{(CL)}$ RESPONSE TO STEP IN $W_{(TL)}$ FOR SECOND ORDER SYSTEM NO. 2,
R_o = 1800 FT.;
$(CT)_g$ = 0.14 SEC.;
$(CT)_c$ = $S_{P(W,P)}$ = 0.640 SEC.

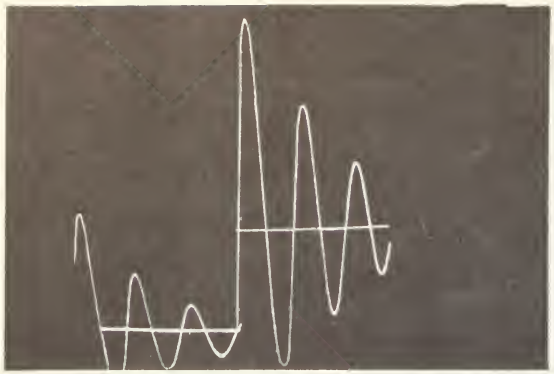

FIG. III-22
$W_{(CL)}$ RESPONSE TO STEP IN $W_{(TL)}$ FOR SECOND ORDER SYSTEM NO. 2,
R_o = 2400 FT.;
$(CT)_g$ = 0.14 SEC.;
$(CT)_c = S_{P(W, P)}$ = 0.938 SEC.

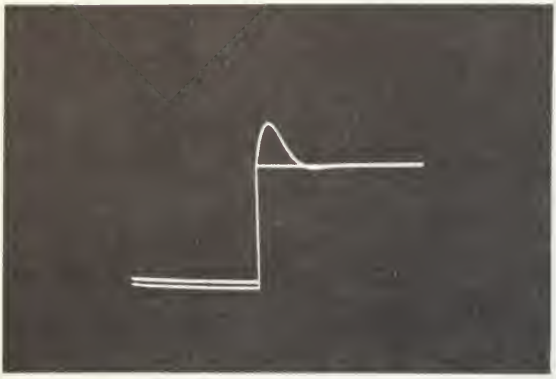

FIG. III-23
$W_{(CL)}$ RESPONSE TO STEP IN $W_{(TL)}$ FOR SECOND ORDER SYSTEM NO. 2,
R_o = 1200 FT.;
$(CT)_g$ = 0.70 SEC.;
$(CT)_c = S_{P(W, P)}$ = 0.375 SEC.

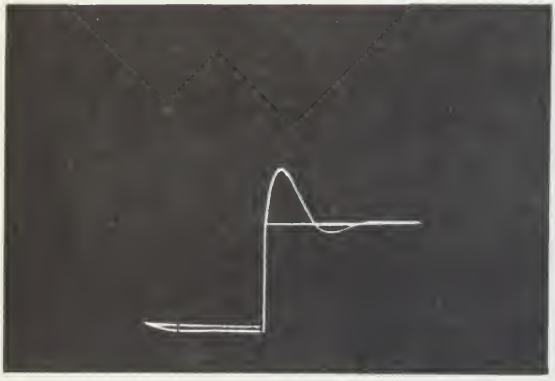

FIG. III-24
$W_{(CL)}$ RESPONSE TO STEP IN $W_{(TL)}$ FOR SECOND ORDER SYSTEM NO. 2,
R_o = 1800 FT.;
$(CT)_g$ = 0.70 SEC.;
$(CT)_c = S_{P(W, P)}$ = 0.640 SEC.

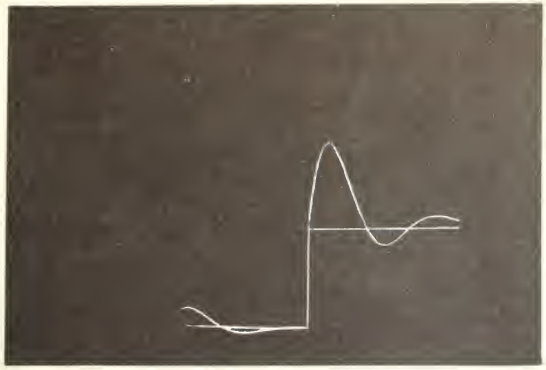

FIG. III-25
$W_{(CL)}$ RESPONSE TO STEP IN $W_{(TL)}$ FOR SECOND ORDER SYSTEM NO. 2,
R_o = 2400 FT.;
$(CT)_g$ = 0.70 SEC.;
$(CT)_c$ = 0.0612 SEC.;
$S_{P(W, P)}$ = 0.14 SEC.

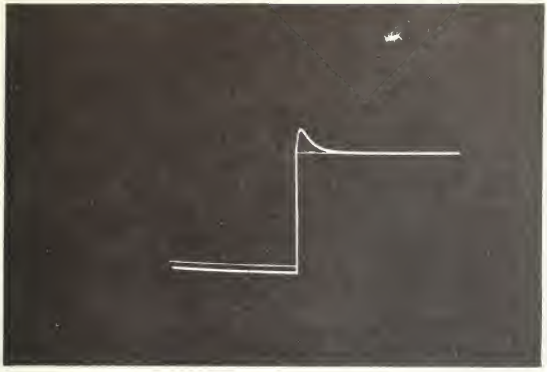

FIG. III-26
$W_{(CL)}$ RESPONSE TO STEP IN $W_{(TL)}$ FOR SECOND ORDER SYSTEM NO. 2,
R_o = 600 FT.;
$(CT)_g$ = 0.70 SEC.;
$(CT)_c$ = 0.0612 SEC.;
$S_{P(W, P)}$ = 0.14 SEC.

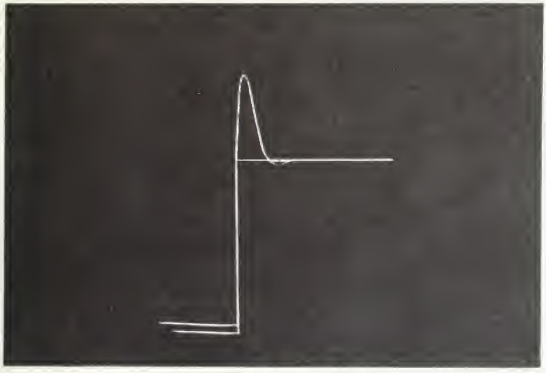

FIG. III-27
$W_{(CL)}$ RESPONSE TO STEP IN $W_{(TL)}$ FOR SECOND ORDER SYSTEM NO. 2,
R_o = 1200 FT.;
$(CT)_g$ = 0.70 SEC.;
$(CT)_c$ = 0.164 SEC.;
$S_{P(W, P)}$ = 0.375 SEC.

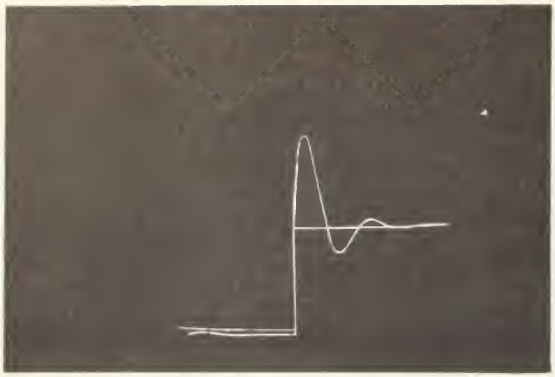

FIG. III-28
$W_{(CL)}$ RESPONSE TO STEP IN $W_{(TL)}$ FOR SECOND ORDER SYSTEM NO. 2,
R_o = 1800 FT.;
$(CT)_g$ = 0.70 SEC.;
$(CT)_c$ = 0.28 SEC.;
$S_{P(W, P)}$ = 0.640 SEC.

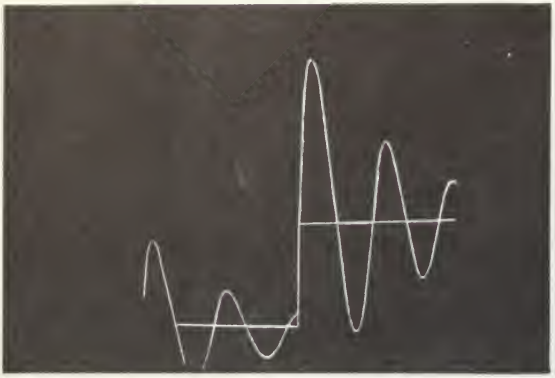

FIG. III-29
$W_{(CL)}$ RESPONSE TO STEP IN $W_{(TL)}$ FOR SECOND ORDER SYSTEM NO. 2,
R_o = 2400 FT.;
$(CT)_g$ = 0.70 SEC.;
$(CT)_c$ = 0.41 SEC.;
$S_{P(W, P)}$ = 0.938 SEC.

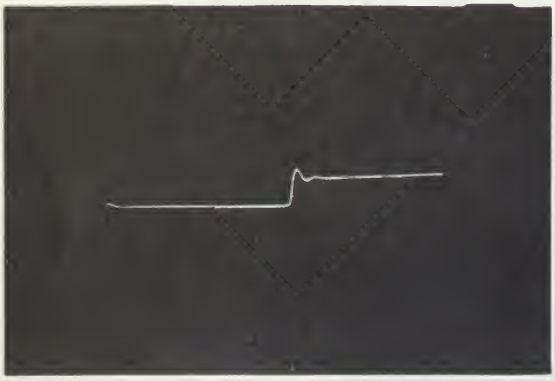

FIG. III-30
P_s RESPONSE TO STEP IN $W_{(TL)}$ FOR SECOND ORDER SYSTEM NO. 2,
R_o = 600 FT.;
$(CT)_g$ = 0.14 SEC.;
$(CT)_c$ = 0.0612 SEC.;
$S_{P(W, P)}$ = 0.140 SEC.

8. Performance of the System for Automatic Tracking.

From the functional diagram of the automatic tracking system, Fig. III-2, it can be seen that the system can be changed from automatic to manual tracking using the double-throw switch as required by the pilot.

For manual tracking, the system has been analyzed in sub-section 6 above. For automatic tracking the system equations are:

$$(C)TL = LS - TL \tag{III-36}$$

$$TL = CL - P_s \tag{III-37}$$

$$CL = [PF]_{LCS(e;CL)}\, e_{(sg)} \tag{III-38}$$

$$e_{(sg)} = S_{(sg)g(A;e)}\, A_g \tag{III-39}$$

$$S_{g(W;M)}\, W_{(CL)} = I_{OA}\, \ddot{A}_g + C_g \dot{A}_g + S_{(tg)g(i^2;M)} i^2_{(tg)} \tag{III-40}$$

$$i^2_{(tg)} = S_{(tg\ amp)(e;i^2)}\, e_{(tk)} \tag{III-41}$$

$$e_{(tk)} = e_{(tsg)} + e_{\dot{P}_s} \tag{III-42}$$

$$e_{(tsg)} = \frac{S_{(t\,cis)(A;e)}\, S_{(tmp)(e;e)}\, [\,1 + (CT)_{tk}\, p]\, (C)TL}{p} \tag{III-43}$$

where

$$(CT)_{tk} = \frac{S_{(tmp)(e;e)}}{S_{(tmi)(\dot{e};e)}} \tag{III-44}$$

$$S_{(tg)c(i^2;M)}\, i^2_{(tg)} = S_{(er)c(A;M)}\, A_c + C_c \dot{A}_c \tag{III-45}$$

$$P_s = S_{i(A;P)}\, A_c \tag{III-46}$$

$$e_{\dot{P}_s} = S_{\dot{P}_s(P;e)}\, p\, P_s \tag{III-47}$$

If $\left(S_{(\text{tg amp})(e;i^2)} [PF]_{g(i^2;e)} [PF]_{(LCS)(e;CL)} [PF]_{\dot{P}_s(W;e)} \right)$

is made equal to 1.0, then the tracking loop is independent of the computer loop. Using this condition and solving the above equations, the following results are obtained:

$$\frac{TL}{(C)TL}$$

$$= \frac{[1 + (CT)_{tk}\, p] S_{(tcis)(A;e)} S_{(tmp)(\dot{e};e)} S_{(\text{tg amp})(e;i^2)} S_{g(W;\dot{e})} [SR]_{(i^2;W)} [PF]_{(LCS)(e;CL)}}{p^2 \left(p\,[(CT)_g\, p + 1] - [PF]_{(LCS)(e;CL)} S_{g(W;\dot{e})} \right)} \qquad \text{(III-48)}$$

Assuming $[PF]_{g(i^2;e)}[PF]_{(LCS)(e;CL)}$ for steady state operation is equal to

$$\frac{S_{g(i^2;e)} S_{(LCS)(e;W)}}{p}$$

$$\frac{CL}{TL} = \frac{[SR]_{(i^2;W)}[(CT)_c\, p + 1]}{[(CT)_c\, p + 1][SR]_{(i^2;W)} - p[SR]_{(i^2;P)}} \qquad \text{(III-49)}$$

Define:

$$S_{P(W,P)} = [SR]_{(W;i^2)} [SR]_{(i^2;P)} \quad \text{as before,}$$

then equation (III-49) becomes,

$$\frac{CL}{TL} = \frac{(SN + 1)\, S_{P(W;P)}\, p + 1}{(SN)\, S_{P(W;P)}\, p + 1} \quad . \qquad \text{(III-50)}$$

Equation (III-50) represents a return to the first order system for which the optimum stability number is again + 0.2. The stability number as defined in equation (III-31) can then be adjusted to optimum setting by varying $[SR]_{(i^2;P)}$ defined in equation (III-11).

Upon examination of Fig. III-2, it is seen that the feedback voltage proportional to $\dot{P}_s$ is necessary in order to effectively separate the tracking loop from the computer and allows the gyro unit to operate in the stabilization channel only. The integration in the

radar circuit is to integrate out any velocity errors that the system picks up and effectively provide smoothing in the circuit.

Due to lack of equipment and time, actual tests were not made with the automatic system, but its similarity to workable existing fire control systems indicates it is an effective and practical system.

9. Conclusions.

For manual tracking, it was shown in the preceding analysis that System No. 2 was unstable at all but the shortest range. In as far as generation of prediction angle was concerned, the system was satisfactory.

In order to obtain stability in manual tracking, several courses may be taken.

First, the characteristic time of the computer can be made equal to $S_{P(W;P)}$ by increasing C_c to 297.5 dyne-cm-sec/mr. The higher damping coefficient could not be obtained with density 2.0 damping fluid, but would require use of density 1.0 damping fluid with consequent redesign of float and case. Additional tracking stability would result from increasing C_g so that $(CT)_g$ would be 0.7 sec. As in the case of the computer, such an increase would require density 1.0 damping fluid and gyro float and case redesign.

A possible second course would be to leave C_c at its current value, and increase C_g to 1220 dyne-cm-sec/mr. Such an increase would again require use of density 1.0 damping fluid and redesign of gyro float and case.

A third alternative involves the insertion into the system of a lead network which exactly cancels the lag term introduced by the gyro. This would lead to effectively a first order system, for which a (SN) of 0.2 would be obtained by increasing C_c to 357 dyne-cm-sec/mr. As in the first alternative, such an increase in C_c would require use of density 1.0 damping fluid and redesign of the computer float and case.

For automatic tracking, it is shown in equation (III-50) that stability in tracking depends chiefly upon the stability number. Since the proper stability number of + 0.2 is not obtainable using the present computer, it is recommended that this unit be redesigned for the use of density 1.0 damping fluid, provided this system is to be given consideration for further study.

CHAPTER IV

CONCLUSIONS AND RECOMMENDATIONS

1. System No. 1

As may be seen from Figs. II-4 and 5 the performance of System No. 1 in generating the proper prediction angle is satisfactory. With the gyro used in the laboratory, however, the system was unsatisfactory for tracking because of low stability number.

In paragraph 6 of Chapter II, the stability number, (SN), was shown to be a function of C_g, $S_{i(A;P)}$, and $S_{g(W;M)}$, as

$$(SN) = \frac{C_g}{S_{g[W;M]} S_{i[A;P]}} - 1$$

and for the system as used in the laboratory (SN) was negative.

Of these quantities, $S_{i(A;P)}$ may be thought of as the "angular gain" between the gimbal shaft and the mirror in the sight head. Since the uncertainty in prediction is the uncertainty of the indicating system plus the product of the uncertainty in gimbal angle and $S_{i(A;P)}$, it was desirable that $S_{i(A;P)}$ be as small as possible. Maximum prediction angle, P_s, is determined by aeroplane geometry, and for current operational fighters is approximately 15^o. In this way $S_{i(A;P)}$ is fixed by maximum P_s and the available gimbal shaft angle and a maximum P_s of 13.2^o, $S_{i(A;P)}$ was 3.77.

With the equipment used in the laboratory, $S_{g(W;M)}$ was $0.1 \times 10^6 \frac{\text{dyne-cm-sec}}{\text{radian}}$ with negligible uncertainty. $S_{g(W;M)}$ could have been reduced to $0.05 \times 10^6 \frac{\text{dyne-cm-sec}}{\text{radian}}$ by use of 200 cps voltage for driving the wheel, but since the uncertainty would have been greater, it was not desirable to do so.

The remaining quantity which could be adjusted to give a (SN) of 0.2, considered optimum for tracking, was the damping coefficient of the gyro, C_g. As is shown in paragraph 6 of Chapter II the C_g required for a (SN) of 0.2 was $.452 \times 10^3$ dyne-cm-sec/mr. Fig. II-6 shows the variation of tracking ratio, TR, with frequency for a C_g of $.452 \times 10^3$ dyne-cm-sec/mr and indicates that under that condition the system is very nearly ideal.

From the results contained in this thesis, it is concluded that the principle employed in System No. 1 is feasible and workable.

If this principle is to be utilized in a redesign of the A-1 Sight, it is recommended that the float and case of the single-degree-of-freedom gyro unit be redesigned so as to enable density 1.0 damping fluid to be used, in order that tracking performance will be satisfactory.

2. System No. 2

It may be seen from Figs. III-6 and III-7, that the performance of System No. 2 in generating the proper prediction angle is satisfactory.

However, with the equipment as set up in the laboratory, the system proved to be unsatisfactory for manual tracking at all but the lowest range due to insufficient system damping.

It has also been shown in this analysis that several courses may be taken in order to remedy this tracking instability in the system.

First, the damping coefficient of the computer can be increased from 130 $\frac{\text{dyne-cm-sec}}{\text{radian}}$ to 297.5 $\frac{\text{dyne-cm-sec}}{\text{radian}}$, and to improve the system stability still further, the damping coefficient of the gyro can be increased from 58.6 $\frac{\text{dyne-cm-sec}}{\text{milliradians}}$ to 293 $\frac{\text{dyne-cm-sec}}{\text{milliradian}}$. Both changes, however, would entail a complete redesign of the units plus the use of density 1.0 damping fluid.

Second, the computer damping coefficient can remain at 130 $\frac{\text{dyne-cm-sec}}{\text{milliradians}}$ provided the gyro damping coefficient were increased to 1220 $\frac{\text{dyne-cm-sec}}{\text{milliradians}}$. This procedure would again mean a redesign of the gyro unit and a shift to density 1.0 damping fluid.

Third, a lead network can be inserted into the system which would cancel the first order lag term introduced by the gyro unit, effectively reducing the system to one of first order. However, for this system to be stable in tracking, the damping coefficient of the computer would have to be increased to 357 dyne-cm-sec/mr, again requiring extensive redesign of equipment. Also smoothing circuits would probably have to be incorporated into the system in order to eliminate noise effects introduced by the insertion of the lead network.

For automatic tracking, the system will be stable provided sufficient damping can be added to the computer unit to provide the proper stability number of + 0.2. Since this is not possible with the present computer, it is recommended that this unit be redesigned for the use of density 1.0 damping fluid, provided it is deemed advisable to give this system further study.

3. General.

System Number 1 as set up in the laboratory was not a satisfactory replacement for the elevation channel of the A-1 Sight, due to tracking instability. With increased damping, however, it is considered that this system would be superior because of greater sensitivity and durability and lighter weight.

For use in a fully automatic system, the configuration of System Number 2 is considered to be workable after the addition of damping.

APPENDIX A

DESCRIPTION OF EQUIPMENT AND COMPONENTS

This Appendix enumerates and completely describes the equipment and components employed in the two fighter aircraft fire control systems analyzed in Chapters II and III. Certain calibration data for these components, necessarily determined for a more complete study, are included.

1. Gyro Unit.

The functional components of the gyro unit include the single-degree-of-freedom gyroscopic element, the microsyn torque generator, the microsyn signal generator and the viscous damper.

Torque from the gyroscopic element is opposed by viscous damping torque due to the relative angular velocity between the float and the gyro case, and by torque fed back through the torque generator. The moving member is floated in damping fluid of density 2 and aligned by pivots in jewel bearings. The small bearing loads resulting from the flotation scheme allow operation at very low friction levels.

This gyro unit is hermetically sealed and thus is free from environmental effects such as dust and humidity. It operates satisfactorily at any temperature from -65°F to 160°F, and warms up to a preset, stabilized temperature in 10 minutes after temperature stabilization in -65°F, ambient. Accelerations up to 10 gravities have no important effect upon operation, while operation with reduced performance will continue up to 100 gravities. Altitude pressure equivalents from sea level to 100,000 feet have no effect upon the operation of the unit. A cutaway drawing of the gyro unit is shown on Fig. A-1.

A brief description and the performance characteristics of the functional components of the gyro unit follow:

a. Microsyn torque generator

The torque generator for this gyro unit is of the 2-inch microsyn type and is a 4-pole electromagnetic device designed to operate on either alternating or direct current. It is connected mechanically to the gyro gimbal shaft and, when supplied with proper excitation, it provides a torque to the roto which is independent of angle, but proportional to the square of the excitation current. A detailed description of this unit appears in Instrumentation Laboratory Engineering Memorandum No. 6411-E-18.

A sensitivity calibration was made on this torque generator and is shown in Table A-1 and Figure A-2. The sensitivity of the

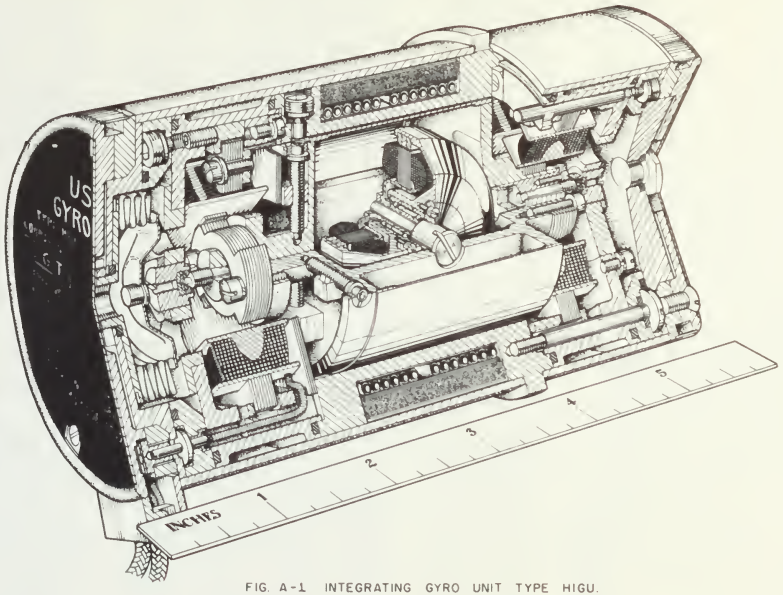

FIG. A-1 INTEGRATING GYRO UNIT TYPE HIGU.

torque generator for current squared in, torque out, was determined by taking the slope of the curve of Figure A-2. This sensitivity, $S_{(tg)g(i^2;\ M)}$, was found to be 40 dyne-cm/$(ma)^2$

b. Microsyn Signal Generator.

The signal generator for this gyro unit is also of the 2-inch microsyn type and is designed to operate at 100 ma, 400 cps excitation current. When operating under these conditions, the sensitivity of the signal generator for angle in, voltage out, is given as 32 millivolts/milliradian by Instrumentation Laboratory Memorandum No. 6411-H-2 (revised). However, by varying the excitation current to a maximum of 400 ma, 1000 cps, the sensitivity may be set at any value up to 300 millivolts/milliradian.

c. Gyroscopic Element

The gyro element of this unit is driven by a 3-phase, 400 cps hysteresis type synchronous motor turning at 12,000 rpm. The operating voltage of this unit is from 10 to 12 volts. The angular momentum of the gyro wheel under these conditions is 105 gram-$(cm)^2$/sec, with other angular momenta possible by varying the speed of the wheel from 6,000 to 12,000 rpm. The moment of inertia of the gyro gimbal assembly is 285 gram-$(cm)^2$.

TABLE A-1 . GYRO UNIT TORQUE GENERATOR SENSITIVITY CALIBRATION

$$M_{(tg)} = S_{g(WM)}\, W_{TT} = 100\, W_{TT}$$

$$S_{(tg)(i^2M)} = \frac{M_{tg}}{i^2} = 40\ \frac{\text{dyne-cm}}{(\text{ma})^2}$$

W_{TT} (mils/sec)	$i_{(tg)}$ (ma)	i_{tg}^2 $(ma)^2$	$M_{(tg)}$ (dyne-cm)
13.09	6	36	1,309
26.18	8	64	2,618
52.36	11.5	132	5,236
104.72	16.1	259	10,472
209.44	23.0	528	20,944

d. Viscous Damper.

Viscous damping is provided by floating the rotating member inside the hermetically sealed case in a damping fluid of density 2. The fluid in this gyro unit has a viscosity of approximately 600 centipoises, providing a damping coefficient of 10^5 dyne-(cm)sec/radian at 160^2F. However, density 2 class fluids are available in a viscosity range of from 0 to 1500 centipoises, permitting selection of damping coefficients from 0 to 250,000 dyne-(cm)sec/radian.

2. Torque Generator Amplifier.

The torque generator amplifier used in the feedback loop was loaned for this study by Mr. J. R. Rogers of the Instrumentation Laboratory. In brief, it consists of a phase-sensitive detector and two parallel channels consisting of a demodulator and a direct current amplifier. Also in each channel is a square root network. The arrangement permits a constant sensitivity for voltage in, current squared out.

This sensitivity was checked, as is shown in Table A-2 and Figure A-3, and was found to be 0.329 $(ma)^2/mv$. It may be seen from Figure A-3 that the current squared is a linear function of the voltage throughout the range of voltages pertinent to the problem.

To insure that the square root networks were linear, the networks for both channels of the amplifier were checked as is shown in Tables A-3 and Figure A-4.

The most important advantage of using this type of amplifier is that the quiescent output is zero, which means that additional friction in the gyro pivots due to side force of the torque generator at zero signal does not exist.

A wiring diagram for the torque generator amplifier is shown in Figure A-5.

3. Computer Unit.

The functional components of the computer unit include two microsyn torque generators, the microsyn elastic restraint generator, the microsyn signal generator and the viscous damper.

Signals received by the input torque generator are opposed by elastic restraint generator torque due to float angular displacement and viscous damping torque due to float angular velocity. Modifying inputs are received through the second torque generator and the elastic restraint generator.

TABLE A-2 . CALIBRATION OF TORQUE GENERATOR AMPLIFIER

$S_{(amp)(e,i^2)(av)} = 0.329 \frac{(ma)^2}{(mv)}$

Counterclockwise Rotation			Clockwise Rotation	
e_{sg} (volts)	i_{tg} (ma)	$i^2_{(tg)}$ $(ma)^2$	i_{tg} (ma)	$i^2_{(tg)}$ $(ma)^2$
.003	.80	.64	1.3	1.69
.01	1.10	1.21	2.3	5.27
.02	2.30	5.27	3.4	11.6
.05	4.2	17.6	5.3	28.0
.07	4.8	23.0	6.1	37.1
.10	5.7	32.4	6.8	46.1
.20	7.7	59.1	8.7	75.4
.50	12.6	158.5	13.2	174
.7	15.0	225	15.3	234
1.0	18.2	331	18.3	334
1.5	22.2	492	22.3	496
2.0	25.7	660	25.4	643
2.5	29.2	852	28.3	800
3.0	32.5	1055	31.4	984

As in the case of the gyro unit, the computer unit operates satisfactorily from temperatures of -65 F to 165 F, acceleration loadings up to 10 gravities, altitude pressure equivalents from sea level to 100,000 feet and is similarly hermetically sealed and thus impervious to dust and humidity. It is likewise temperature stabilized, and reaches preset operating temperature in ten minutes.

A cutaway drawing of the computer is shown in Figure A-6 and an exploded view photograph appears as Figure A-7.

A brief description and the performance characteristics of the functional components of the computer unit follow:

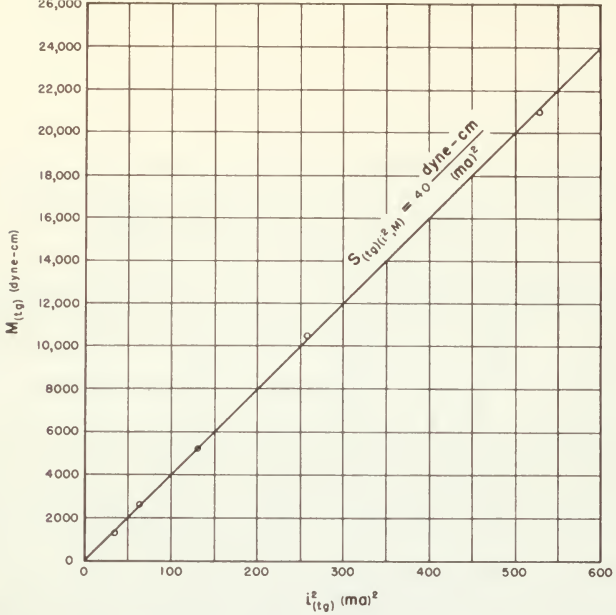

FIG. A-2. GYRO UNIT TORQUE GENERATOR SENSITIVITY CALIBRATION.

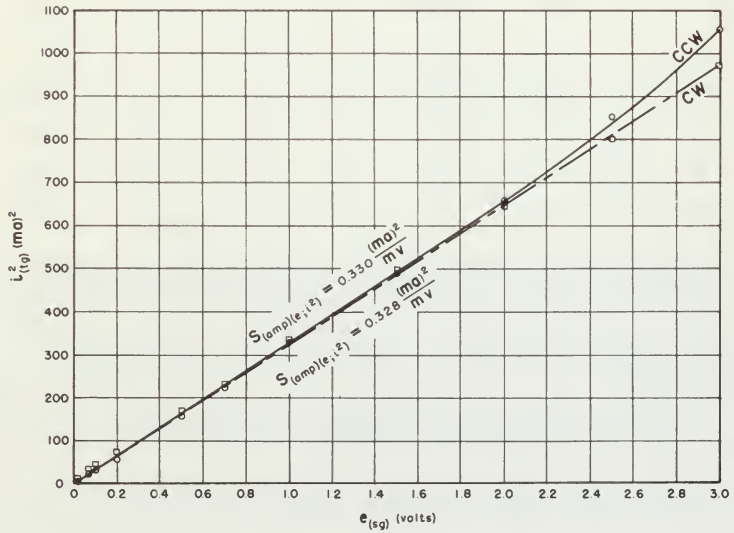

FIG. A-3. CALIBRATION OF TORQUE GENERATOR AMPLIFIER.

a. Microsyn Torque Generator.

The torque generator for the computer unit is essentially the same as that for the gyro unit, so a repetition of its description and operation will not be necessary. The principal difference in the torque generator units is in their sensitivities, the sensitivity of the computer torque generator being given as 38.3 dyne-(cm)/(ma)^2 by Instrumentation Laboratory Memorandum No. 6411-H-9. The other torque generator in the computer has still a different sensitivity, but it was not used in this study.

b. Microsyn Elastic Restraint Generator.

As in the case of the torque generator and signal generator previously described, the elastic restraint generator is a four-pole, electromagnetic device of the 2-inch microsyn type connected

TABLE A-3 . CALIBRATION OF SQUARE ROOT NETWORK

Channel 1		Channel 2	
e_{in} (volts)	e_{out} (volts)	e_{in} (volts)	e_{out} (volts)
18.5	2.1	13	1.95
29	2.65	26.5	2.75
39.5	3.1	35.5	3.15
50	3.45	44	3.5
61.5	3.8	54	3.9
73	4.2	65	4.2
83.5	4.5	74	4.5
92	4.75	83.5	4.8
11.5	1.6	93.5	5.1
4.8	1.1		

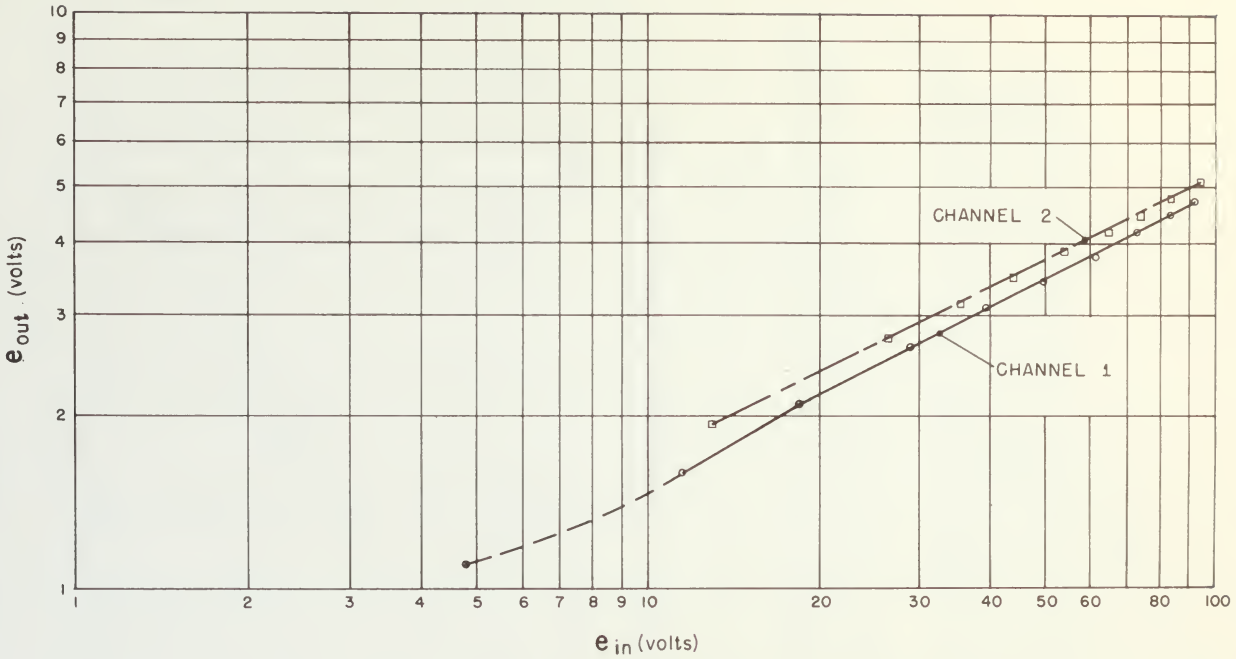

FIG. A-4. CALIBRATION OF SQUARE ROOT NETWORKS FOR TORQUE GENERATOR AMPLIFIER

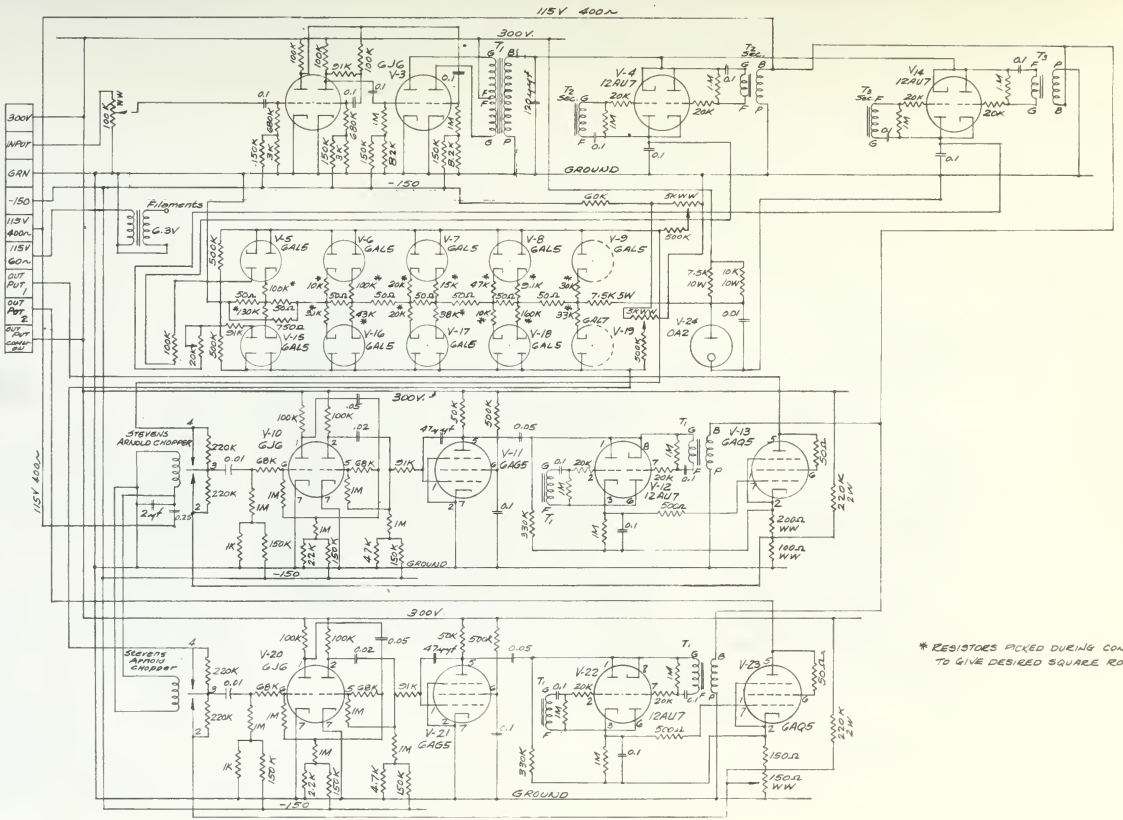

FIG. A-5 TORQUE GENERATOR AMPLIFIER

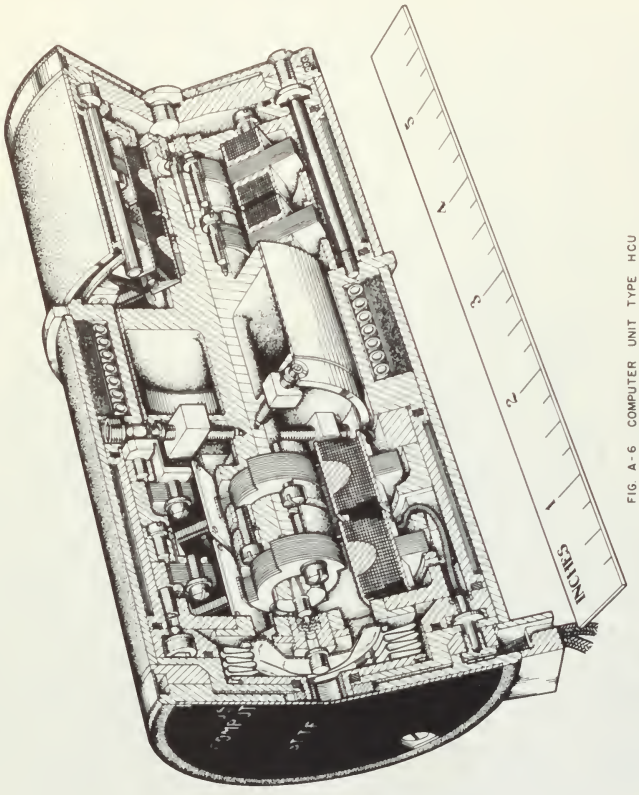

FIG A-6 COMPUTER UNIT TYPE HCU

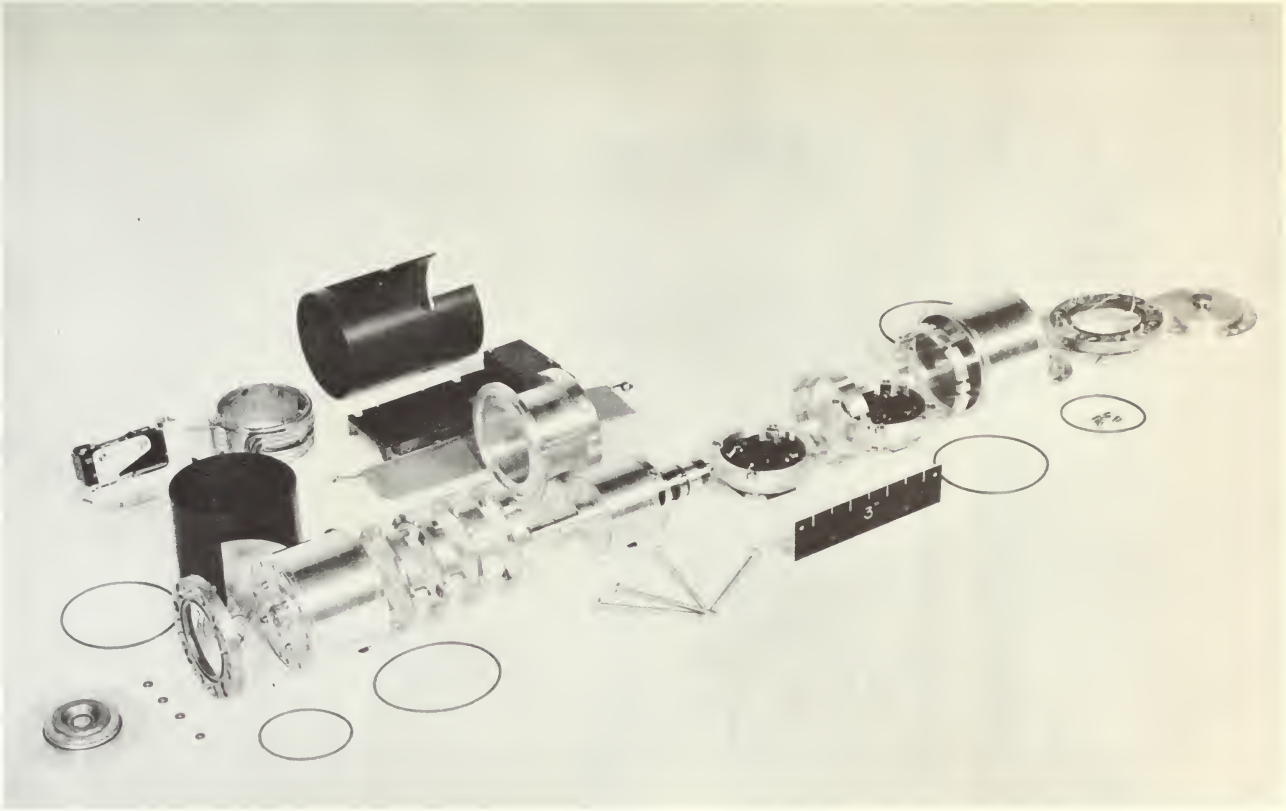

FIG. A-7. COMPUTER UNIT.

directly to the computer shaft. When supplied with the proper excitation, it provides a restraint proportional to angular displacement and to the square of the excitation current. A more detailed description of this unit appears in Instrumentation Laboratory Engineering Memorandum No. 6411-E-17.

The sensitivity of this unit is given as 0.25 dyne-(cm)/mr-$(ma)^2$ by Instrumentation Laboratory Memorandum No. 6411-H-9.

The elastic restraint generator was used as a range input to the system as is described in Chapter III of this analysis.

c. Microsyn Signal Generator.

The signal generator for the computer unit is essentially the same as that for the gyro unit, so a repetition of its description and operation will not be necessary. The principal difference in the two is in their sensitivities, the sensitivity of the computer signal generator being given as 27.5 mv/mr at 100-ma, 400-cps excitation current by Instrumentation Laboratory Memorandum Number 6411-H-9.

d. Viscous Damper.

Viscous damping in the computer is provided in the same manner as in the gyro unit. However, the viscosity of the damping fluid in the computer was 1700 centipoises, providing a damping coefficient of 1.1×10^5 dyne-cm-sec/radian at 160° F.

APPENDIX B

REFERENCES

1. Instrumentation Laboratory of the Massachusetts Institute of Technology: Detailed Theory and Computations for the A-1 Sight for the Control of Gunfire from Fixed Guns, Rocketfire, and Bombing from Aircraft, Vols. I and II, 1945-1946.

2. Feldman, J.B.: "Progress Report on A-1 Rocket Sight", Engineering Memorandum No. 6411-P-1, 22 May 1947.

3. Haskell, C.A.: "Specifications and Performance Characteristics of 2-inch Microsyn Torque Generator", Engineering Memorandum No. 6411-E-18, 7 December 1949.

4. Haskell, C.A.: "USAF Computer Unit HCU-ST-TE", Engineering Memorandum No. 6411-E-22, 17 February 1950.

5. Haskell, C.A.: "USAF Integrating Gyro HIGU, Performance Characteristics and Specifications", Engineering Memorandum No. 6411-H-2 (revised), 30 December 1949.

APPENDIX C

GLOSSARY OF SYMBOLS AND TERMS

The system of notation adopted for use in this thesis has been selected because it fulfills the following desirable objectives:

1. It is easily learned.

2. It is adaptable to a wide range of situations.

3. It is built up almost exclusively of characters found on the keyboard of a standard American typewriter.

4. Any one of the compound symbols of the system is readily interpreted without recourse to an extensive glossary.

A few simple examples suffice to explain the operation of the notation system. These examples are shown in Table C-3. The short table of key symbols given at the end of the explanation will then furnish sufficient information to enable any compound symbol to be correctly interpreted, and to provide the necessary tools for the generation of new symbols.

The symbology used throughout is intended to agree with the system of notation originated by Dr. C. S. Draper of the Instrumentation Laboratory at the Massachusetts Institute of Technology.

TABLE C-1

PRIMARY SYMBOLS

A	Angle	p	Heaviside operator
C	Damping Coefficient	R	Range
CL	Control Line	R_o	Present range
(CT)	Characteristic Time	S	Sensitivity
(DR)	Damping Ratio	(SN)	Stability number
e	Voltage	TL	Tracking Line
i	Current	(TR)	Tracking Ratio
H	Angular Momentum	t	Time
M	Torque	W	Angular velocity
P_s	Prediction angle		

TABLE C-2

MODIFYING SYMBOLS (SUBSCRIPTS)

(amp)	Amplifier
c	Computer
g	Gyro
i	Indicating System
l	Linkage
m	Mirror
(sg)	Signal Generator
(tg)	Torque Generator
(tg amp)	Torque Generator Amplifier

TABLE C-3

TYPICAL EXAMPLES SHOWING HOW SYMBOLS ARE COMPOUNDED FROM THE ELEMENTARY FORMS

$S_{i(A;P)}$	Sensitivity of the indicating system for angle in, prediction angle out
$S_{P(W;P)}$	Sensitivity of prediction system for angular velocity in, prediction angle out
$(CT)_c$	Characteristic time of the computer

APPENDIX D

LIST OF EQUIPMENT

1	Rate Table
1	Single-Degree-Of-Freedom Gyro Unit, Serial No. 2.
1	USAF Computer Unit, Serial No. 142.
1	AAF A-1 Sight Head, Serial No. 665096.
1	AAF A-1 Sight Servo Amplifier, Serial No. 665098.
1	Torque Generator Amplifier.
1	Stromberg-Carlson Linear Amplifier, Serial No. 411-288.
2	Stromberg-Carlson Linear Amplifier, Model AU-34.
1	Pioneer Autosyn, Serial No. AY-14-G.
1	300 Volt, dc B supply, Serial No. 505-501.
1	400 cps Vacuum Tube Fork, Serial No. 673.
1	Kenyon 3-Phase Transformer, Serial No. S 23939.
1	Bogen Linear Amplifier, model PH-10.
1	Phase Shifting Network.
1	Vacuum Tube Voltmeter, Serial No. 411-297.
1	Cornell Dubilier Decade Capacitor, Serial No. 411-248.
1	Variac.
1	AC Milliameter, Serial No. 77070.
1	GAP/R Electronic Simulator.
	Various Simpson Voltmeter-Ohmeter-Milliameters, Dumont Cathode Ray Oscilloscopes and Test Equipment.

APPENDIX E

SENSITIVITY DATA

This appendix contains the tables of data from which are plotted the sensitivity curves in Chapters II and III.

TABLE II-1

DETERMINATION OF $S_{i(e;P)}$ SYSTEM NO. 1	
e_{sg} (volts)	P_s (mr)
+ .05	1
- .05	3
+ .10	8
- .14	19
+ .225	22
- .325	41
+ .50	55
- .64	77
+1.03	121
-1.50	177

TABLE II-2

PREDICTION PERFORMANCE OF SYSTEM NO. 1						
R_o (feet)	1200		1800		2400	
$W_{(CL)}$ (mr/sec)	P_s (mr)	$P_{s(corr)}$ (mr)	P_s (mr)	$P_{s(corr)}$ (mr)	P_s (mr)	$P_{s(corr)}$ (mr)
6.545	2.0	2.5	4	4.2	6	6.2
13.09	5.0	4.9	8	8.4	11	12.3
26.18	10	9.8	16.5	16.7	25	24.5
52.36	19	19.6	33	33.5	50	49
104.72	39.5	39.2	68	67	110	98
209.44	78.5	78.4	136	134	—	--

TABLE II-3

TRACKING RATIO Vs TRACKING FREQUENCY FOR SYSTEM NO. 1

$C_g = .058 \times 10^3$ AND $C_g = .452 \times 10^3 \frac{\text{dyne-cm-sec}}{(\text{mr})}$

W_{TR} (mr/sec)	$C_g = .058 \times 10^3 \frac{\text{dyne-cm-sec}}{(\text{mr})}$ TR	$C_g = .452 \times 10^3 \frac{\text{dyne-cm-sec}}{(\text{mr})}$ TR
0	1.0	1.0
10	0.35	3.69
20	0.24	5.04
50	0.194	5.8
100	0.187	5.96
200	0.184	6.0
400	0.184	6.0

TABLE III-1

DETERMINATION OF $S_{i[e;P]}$ FOR SYSTEM 2				
	CLOCKWISE ROTATION		COUNTERCLOCKWISE ROTATION	
W_{TT} (mils/sec)	Ps (mils)	e (mv)	Ps (mils)	e (mv)
6.545	3	30	3	38
13.09	9	90	6	68
26.18	19	170	16	160
52.36	37	320	36	330
104.72	79	690	77	690
209.44	163	1400	157	1400
$S_{i[e;P]}$ 0.113 $\frac{\text{milliradians}}{\text{millivolt}}$				

TABLE III-2

SENSITIVITIES, CHARACTERISTICS TIMES AND COEFFICIENTS FOR THE ANALYSIS OF SYSTEM NO. 2

$C_g = 58.6 \frac{\text{dyne-cm-sec}}{\text{milliradian}}$

$C_c = 130.0 \frac{\text{dyne-cm-sec}}{\text{milliradian}}$

$S_{g(W,M)} = H = 100 \frac{\text{dyne-cm-sec}}{\text{milliradian}}$

$S_{(tg)g(i^2,M)} = 40 \frac{\text{dyne-cm}}{(\text{ma})^2}$

$S_{(tg)c(i^2,M)} = 38.3 \frac{\text{dyne-cm}}{(\text{ma})^2}$

$S_{(sg)g(A,e)} = 32 \frac{\text{millivolt}}{\text{milliradian}}$ (at 100 ma excitation)

$S_{(sg)c(A,e)} = 27.5 \frac{\text{millivolt}}{\text{milliradian}}$ (at 100 ma excitation)

$S_{(er)c(A,i^2;M)} = 0.25 \frac{\text{dyne-cm}}{\text{milliradian-}(\text{ma})^2}$

$S_{i(e;P)} = 0.113 \frac{\text{milliradians}}{\text{millivolt}}$

$S_{i(A,P)} = 3.11$

$S_{(tg\ amp)(e,i^2)} = 0.329 \frac{(\text{ma})^2}{\text{millivolt}}$

$(CT)_g = 0.1395$ secs.

$(CT)_c = \frac{520}{i^2_{(er)}}$ secs.

$S_{P(W,P)} = \frac{1190}{i^2_{(er)}}$ secs.

TABLE III-3

(AR) AND (PA) OF $\frac{P_s}{W_{(OL)}S_{p(W,P)}}$ VERSUS W FOR R_o = 6000 FEET AT SEA LEVEL

$i^2(er) = 276(ma)^2$	$(CT)_g = .1395$ secs.	$(CT)_c = 1.882$ secs.
W (rad/sec)	(AR)	PA (degrees)
.05	1.0	-5
.10	.975	-11
.2	.931	-21
.5	.74	-45
.7	.60	-57
1.0	.467	-69
2	.245	-92
5	.089	-120
7	.055	-131
10	.032	-142
20	.009	-159
30	.004	-167
40	.002	-171

TABLE III-4

(AR) AND (PA) OF $\frac{P_s}{W_{(CL)} S_{p(W,P)}}$ VERSUS

W FOR R_o = 3000 FEET AT SEA LEVEL

$i^2_{(er)} = 919\ (ma)^2$ $(CT)_g = .1395$ secs. $(CT)_o = .566$ secs.

W(rad/sec)	(AR)	(PA) (degrees)
.05	1.0	-1
.10	1.0	-2
.2	.975	-7
.5	.95	-20
.7	.931	-27
1.0	.85	-37
2	.63	-63
5	.275	-105
7	.17	-120
10	.10	-134
20	.029	-154
30	.013	-163
40	.007	-169

TABLE III-5

(AR) AND (PA) OF $\frac{P_s}{W(CL)S_{p(W,P)}}$ VERSUS W FOR R_o = 1200 FEET AT SEA LEVEL

$i^2_{(er)} = 3175\ (ma)^2$ $(CT)_g = .1395$ secs $(CT)_o = .164$

W (rad/sec)	(AR)	(PA) (degrees)
.05	1.0	0
.1	1.0	0
.2	1.0	-1
.5	1.0	-7
.7	1.0	-12
1.0	.975	-17
2	.91	-34
5	.63	-72
7	.47	-91
10	.3	-110
20	.1	-143
30	.046	-157
40	.025	-163

TABLE III-6

P_s vs. W_{ig} FOR VARIOUS RANGES AT SEA LEVEL

$i^2(er)$ $(ma)^2$	3175		1860		1270		919		430		276	
R_o (feet)	1200		1800		2400		3000		4800		6000	
$W_{(CL)}$ (mils/sec)	P_s (mils)	$P_{s(corr)}$ (mils)	P_s (mils)	$P_{s(corr)}$ (mils)	P_s (mils)	$P_{s(corr)}$ (mils)	P_s (mils)	$P_{s(corr)}$ (mils)	P_s (mils)	$P_{s(corr)}$ (mils)	P_s (mils)	$P_{s(corr)}$ (mils)
6.545	2.0	2.5	3.5	4.2	5.0	6.2	7.6	8.5	14.0	18.1	24.0	28.2
13.09	5.0	4.9	7.0	8.4	11.5	12.3	15.0	16.9	33.5	36.2	53.0	56.4
26.18	9.0	9.8	15.0	16.7	23.0	24.5	33.5	33.9	70.0	72.4	107.0	112.8
52.36	19.0	19.6	33.0	33.0	49.5	49.0	66.0	67.8	143.0	144.7	225.0	225.6
104.72	41.0	39.2	68.0	67.0	103.5	98.0	137.0	135.6	Hit Stop		Hit Stop	
209.44	84.5	78.4	141.0	134.0	213.0	196.0	Hit Stop		Hit Stop		Hit Stop	

TABLE III-7

P_s vs. W_{ig} FOR VARIOUS RANGES AT 16,000 FT.												
i^2(er) $(ma)^2$	3240		2145		1465		1072		554		406	
R_o (feet)	1200		1800		2400		3000		4800		6000	
$W_{(CL)}$ (mils/sec)	P_s (mils)	$P_{s(corr)}$ (mils)	P_s (mils)	$P_{s(corr)}$ (mils)	P_s (mils)	$P_{s(corr)}$ (mils)	P_s (mils)	$P_{s(corr)}$ (mils)	P_s (mils)	$P_{s(corr)}$ (mils)	P_s (mils)	$P_{s(corr)}$ (mils)
6.545	2.5	2.4	3.5	3.6	5.0	5.3	6.0	7.3	13.0	14.0	18.0	19.2
13.09	4.6	4.8	6.5	7.3	9.0	10.6	13.0	14.5	27.0	28.1	36.0	38.4
26.18	9.5	9.6	14.0	14.5	19.5	21.2	27.5	29.0	55.0	56.2	77.0	76.8
52.36	19.5	19.2	29.0	29.0	42.0	42.4	58.0	58.0	112.0	112.4	154.5	152.6
104.72	41.0	38.4	60.0	58.0	86.0	84.8	120.0	116.0	228.5	224.8	Hit Stop	
209.44	85.0	76.8	124.5	116.0	177.0	169.6	Hit Stop		Hit Stop		Hit Stop	

TABLE III-8

$(AR)_{(CL-TL)}$ Vs, W FOR VARIOUS RANGES AT SEA LEVEL - SYSTEM NO. 2			
W (rad/sec)	$(AR)_{(CL-TL)}$ R_o = 6000 ft.	$(AR)_{(CL-TL)}$ R_o = 3000 ft.	$(AR)_{(CL-TL)}$ R_o = 1200 ft.
0.1	1.000	1.000	1.000
0.5	1.080	0.982	0.990
1	1.119	0.945	0.957
2	1.136	0.873	0.840
3			0.680
5	1.110	0.850	0.354
6			0.256
7			0.242
10	1.053	0.920	0.447
20	1.020	0.973	0.815
40	1.005	0.993	0.946
70	1.000	0.998	0.983
100	1.000	0.999	0.992

TABLE III-9

(DRR) Vs. R_o AT SEA LEVEL FOR

$(CT)_c = \left(\frac{520}{i^2_{(er)}}\right)$ SECONDS, $(CT)_g = 0.1375$ SECONDS

$S_{p(W,P)} = \frac{1190}{i^2_{(er)}}$ SECONDS

R_o (ft.)	$i^2_{(er)}$ $(ma)^2$	$(CT)_c$ (secs)	$(CT)_g + (CT)_c$ (secs)	$S_{p(W,P)}$ (secs)	(DRR)
600	8500	.0612	.2007	.140	+ .300
1200	3175	.164	.3035	.375	- .240
1800	1860	.280	.4200	.640	- .523
2400	1270	.410	.5500	.938	- .708
3000	919	.566	.7060	1.295	- .834
3600	706	.737	.8770	1.685	- .920
4200	540	.964	1.104	2.200	- .992
4800	430	1.210	1.350	2.770	-1.050
5400	344	1.510	1.650	3.460	-1.100
6000	276	1.885	2.025	4.313	-1.130

TABLE III-10

(DRR) Vs. R_o AT SEA LEVEL FOR

$(CT)_c = S_{p(W,P)} = \frac{1190}{i^2_{(er)}}$ SECONDS; $(CT)_g$ = 0.1395 SECONDS

R_o (ft.)	$i^2_{(er)}$ $(ma)^2$	$(CT)_c = S_{p(W,P)}$ (secs)	$(CT)_g + (CT)_c$ (secs)	(DRR)
600	8500	.140	.2795	+.500
1200	3175	.375	.5150	.271
1800	1860	.640	.780	.180
2400	1270	.938	1.078	.130
3000	919	1.295	1.435	.097
3600	706	1.685	1.825	.077
4200	540	2.200	2.340	.060
4800	430	2.770	2.910	.047
5400	344	3.460	3.600	.038
6000	276	4.313	4.450	.031